International Journal of Solids and Structures 174–175 (2019) 1–17

Contents lists available at ScienceDirect

International Journal of Solids and Structures

journal homepage: www.elsevier.com/locate/ijsolstr

Localization analysis of nonlocal models with damage-dependent nonlocal interaction

Milan Jirásek[a,*], Rodrigue Desmorat[b]

[a] Czech Technical University in Prague, Faculty of Civil Engineering, Department of Mechanics, Thákurova 7, Prague 6 16629, Czech Republic
[b] LMT, ENS Paris-Saclay/CNRS/Université Paris-Saclay, 61 avenue du Président Wilson, Cachan Cedex F-94235, France

ARTICLE INFO

Article history:
Received 4 February 2019
Revised 28 May 2019
Accepted 10 June 2019
Available online 14 June 2019

Keywords:
Damage mechanics
Plasticity
Strain localization
Softening
Nonlocal models

ABSTRACT

This paper systematically evaluates (in the one-dimensional setting) the performance of a new type of integral nonlocal averaging scheme, initially motivated by the idea of internal time that reflects the reduction of the elastic wave speed in a damaged material. The formulation dealing with internal time is replaced by the equivalent concept of a modified spatial metric leading to a damage-dependent interaction distance. This modification has a favorable effect on the evolution of the active part of damage zone and leads to its gradual shrinking, which naturally describes the transition from a thin process zone to a fully localized crack. However, when a pure damage model (with no permanent strain) is considered, the resulting load-displacement diagrams exhibit dramatic snapbacks and excessively brittle behavior in the final stages of failure. The concept of damage-dependent interaction distances is therefore extended to damage-plastic models and damage models with inelastic (permanent) strain. It is shown that, for formulations that consider a part of the strain as irreversible, the overall stress-displacement response becomes realistic for quasi-brittle materials such as concrete, for which the diagram typically exhibits a long tail.

1. Introduction

Integral-type nonlocal formulations of material models with stress softening are usually based on weighted spatial averaging with a fixed weight function that depends on the standard geometric distance between interacting material points (Pijaudier-Cabot and Bažant, 1987; Bažant and Jirásek, 2002). Arguments explaining the physical motivation for nonlocal averaging have been advanced for instance in Bažant (1990, 1994), Bažant and Jirásek (1994). These studies attempt homogenization of the deformations caused by micro-cracks in an elastic solid and indicate that non-locality already occurs for dilute homogenization schemes and is enhanced by the interactions among microcracks. Differences in the approach to geometrical modeling of the material microstructure may lead to different implications for the evolution of the internal length. Some theories suggest that, at small microcrack density, the internal length increases due to the porosity effect (Pijaudier-Cabot et al., 2004) or due to the boundary effect (Krayani et al., 2009).

The nonlocal formulations act as efficient localization limiters and provide an objective description of strain localization. They lead to proper convergence of numerical solutions to meaningful limits characterized by finite energy dissipation (Pijaudier-Cabot and Benallal, 1993). However, certain deficiencies of the nonlocal formulations have been identified (Geers et al., 1998; Jirásek et al., 2004; Simone et al., 2004; Krayani et al., 2009; Bažant et al., 2010; Giry et al., 2011; Grégoire et al., 2013).

Starting from the pioneering works (Pijaudier-Cabot and Bažant, 1987; Peerlings et al., 1996), the characteristic length has usually been assumed as constant. In reality, it has to evolve (Geers et al., 1998), which is a fact confirmed by micro-mechanics analyses (Pijaudier-Cabot et al., 2004; Krayani et al., 2009; Sun and Poh, 2016). A related difficult point is proper modeling of the boundary effect (Bažant et al., 2010; Krayani et al., 2009; Giry et al., 2011). The propagation of a crack modeled as a localized damaged band may not start directly from an existing crack tip in a pre-cracked structure but rather from a point located at a finite distance from the tip (Simone et al., 2004). Furthermore, size effects may be misrepresented (Jirásek et al., 2004; Grégoire et al., 2013) and nonlocal integral weight functions may become non-symmetric due to boundary effects (Borino et al., 2003).

Another problematic aspect is that, physically, material points located on the opposite sides of a stress-free crack should not

* Corresponding author.
E-mail addresses: milan.jirasek@fsv.cvut.cz (M. Jirásek), desmorat@lmt.ens-cachan.fr (R. Desmorat).

https://doi.org/10.1016/j.ijsolstr.2019.06.011
0020-7683/

interact even if their geometric distance is small. This natural requirement can be taken into account for a pre-existing crack (or notch), e.g., by defining the interaction distance based on the shortest path that does not cross the crack (such as in the visibility check method (Belytschko et al., 1995; 1996)). However, such an adjustment captures only pre-existing cracks and does not reflect the effects of a growing process zone that eventually develops into a new stress-free segment. Another deficiency of the standard averaging techniques is that, when applied to models with damage driven by the nonlocal equivalent strain, they lead to a spurious expansion of the damage profile at late stages of the failure process (Bažant and Pijaudier-Cabot, 1988).

The nonlocal (or gradient/phase field) damage models with an evolving internal length introduced by a number of authors (Frémond and Nedjar, 1996; Geers et al., 1998; Simone et al., 2003; Pijaudier-Cabot et al., 2004; Miehe et al., 2010; Pijaudier-Cabot and Dufour, 2010; Desmorat et al., 2010; Nguyen, 2011; Saroukhani et al., 2013) could potentially be useful for modeling of a progressive transition from diffuse damage to strain localization by bridging Continuum Damage Mechanics and Fracture Mechanics, reflecting the natural expectation that the nonlocal interactions get weaker (up to vanishing) when the internal length decreases. The works cited above are based on different physics; they include pure phenomenological (Geers et al., 1998; Simone et al., 2003; Desmorat et al., 2010; Saroukhani et al., 2013) and thermodynamically consistent (Frémond and Nedjar, 1996; Miehe et al., 2010; Nguyen, 2011) approaches as well as micro-mechanics based ones (Pijaudier-Cabot et al., 2004; Pijaudier-Cabot and Dufour, 2010).

The objective of this paper is to systematically compare and evaluate the performance of a new type of nonlocal averaging (Desmorat et al., 2015), initially motivated by the idea of internal time that reflects the reduction of the elastic wave speed in a damaged material (Desmorat and Gatuingt, 2007; 2010). Instead of internal time, one can equivalently consider a modified spatial metric leading, in a uniformly damaged body, to a damage-dependent interaction distance (or effective distance) locally defined as the standard geometric distance divided by the square root (in terms of principal values) of the integrity tensor. In the one-dimensional (1D) non-uniform case, the effective distance $\tilde{r}(x_1, x_2) = \tilde{r}(x_2, x_1)$ between two points of abscissa x_1 and x_2 is defined by (Desmorat and Gatuingt, 2007)

$$\tilde{r}(x_1, x_2) = \int_{\eta=\min(x_1,x_2)}^{\max(x_1,x_2)} \frac{\mathrm{d}\eta}{\sqrt{1 - D(\eta)}}, \tag{1}$$

where D is the damage variable. Previous studies indicated that this approach leads to a nice shrinking of the active part of damage zone, which naturally describes the transition to a fully localized crack (Desmorat et al., 2015; Rastiello et al., 2018). However, the resulting load-displacement diagrams exhibit dramatic snapbacks and excessively brittle behavior in the final stages of failure.

A known feature of concrete, not captured by the so-called pure damage models, is that it exhibits permanent strains (Terrien, 1980; Mazars et al., 1989; 1990; Ragueneau et al., 2000), caused partially by imperfect crack closure and by dissipative processes related to crack friction. A first modeling framework is the theory of plasticity, coupled with damage in the so-called Damage-Plastic Models in the same way as in Govindjee et al. (1995), Feenstra and Borst (1996), Meschke et al. (1998), Burlion et al. (2000), Nechnech et al. (2002), Grassl and Jirásek (2006). A second modeling possibility is to follow Hermann and Kestin (1988) and to model permanent strains as caused by damage (either isotropic (Borderie, 1991) or anisotropic (Halm and Dragon, 1998; Desmorat, 2004; Lebon, 2011), see also Matallah and Borderie, 2009) in constitutive models with damage-driven inelastic strain. In the present contribution, the concept of damage-dependent interaction distances is extended from pure damage models (DM) to damage-plastic models (DPM) and damage models with inelastic (permanent) strain (DMIS). Localization behavior is studied here in 1D, which is sufficient for evaluation of the basic characteristics of the process zone and load-displacement diagram. In multiple dimensions, computation of effective distances will require much more effort, and only promising formulations that pass the basic 1D test will be selected for extension to a more general setting.

2. Local models—Basic equations

2.1. Common framework

Nonlocal averaging with damage-dependent interaction distance is in general applicable to any type of continuum damage model, but for the present purpose it is sufficient to restrict attention to isotropic models with a single scalar damage variable D. Such models use the stress-strain law in the form (Lemaitre and Chaboche, 1985)

$$\boldsymbol{\sigma} = (1 - D)\mathbf{E} : \boldsymbol{\varepsilon} \tag{2}$$

where $\boldsymbol{\sigma}$ is the stress tensor, $\boldsymbol{\varepsilon}$ is the strain tensor, and $\mathbf{E}$ is the elastic stiffness tensor. The damage variable D grows from 0 for the initially intact material to 1 for the fully damaged material and its growth is usually driven by a suitably defined scalar measure of strain called the equivalent strain. The choice of a specific expression for equivalent strain affects the shape of the elastic domain in the strain space and thus indirectly also in the stress space. The simplest choices based on the tensorial strain norm or elastic energy density (Marigo, 1981) would lead to a symmetric behavior in tension and in compression and therefore are not suitable for quasibrittle materials. Definitions that take into account easier damage growth under tension include the modified Mises definition (de Vree et al., 1995), Mazars (1984), standard or smooth Rankine and other specifically adjusted expressions.

In the present paper, only one-dimensional tensile response is considered, and so (2) simplifies to

$$\sigma = (1 - D)E\varepsilon \tag{3}$$

where σ is the axial stress, ε is the axial strain, and E is Young's modulus. The equivalent strain is then equal to the axial strain. Under monotonic tensile loading, the damage variable can be directly linked to the (equivalent) strain by a certain non-decreasing function g. The simplest form of the damage law is thus

$$D = g(\varepsilon) \tag{4}$$

The specific form of damage function g can be derived from the uniaxial stress-strain diagram. For instance, to obtain a stress-strain diagram with linear elasticity up to the peak stress f_t, followed by exponential softening, one needs to set

$$g(\varepsilon) = \begin{cases} 0 & \text{for } \varepsilon \le \varepsilon_0 \\ 1 - \dfrac{\varepsilon_0}{\varepsilon} \exp\left(-\dfrac{\varepsilon - \varepsilon_0}{\varepsilon_f - \varepsilon_0}\right) & \text{for } \varepsilon > \varepsilon_0 \end{cases} \tag{5}$$

where $\varepsilon_0 = f_t/E$ is the limit elastic strain and ε_f is a parameter that controls the steepness of the softening branch.

In previous studies it was found that, for a pure damage model with a local damage law that corresponds to exponential softening, the enhancement by a nonlocal formulation with interaction distance proportional to $1/\sqrt{1 - D}$ (by Eq. (1)) leads to an excessively brittle global response, especially at late stages of the localization process (Desmorat et al., 2015). One of the main objectives of the present paper is to determine which particular models enhanced by the nonlocal formulation with damage-dependent interaction distance would lead to a global response characterized by load-displacement diagrams with a relatively long tail, which is

typically found in experiments for concrete and similar quasi-brittle materials; see Section 4.2 for a specific example and detailed discussion.

It can be expected that the global response is affected not only by the local damage law but also by the nature of the underlying model. For instance, if the model is enriched by inelastic strains, damage evolution is slowed down and this might have a favorable effect on the shape of the load-displacement diagram. Therefore, in our comparative study, we consider the uniaxial stress-strain law in a more general form

$$\sigma = (1-D)E(\varepsilon - \varepsilon_p) \tag{6}$$

where ε_p is the inelastic (or plastic) strain. To describe the evolution of damage in a general case (not restricted to monotonic loading), a simple dependence of damage on strain is replaced by Kuhn–Tucker loading-unloading conditions

$$f_d(\kappa_d, \ldots) \le 0, \qquad \dot\kappa_d \ge 0, \qquad f_d(\kappa_d, \ldots)\,\dot\kappa_d = 0 \tag{7}$$

in which κ_d is the damage-driving variable, f_d is the damage loading function (which depends not only on κ_d but also on additional variables, to be specified later), and the superimposed dot denotes the time derivative. The specific definition of f_d and κ_d depends on the considered type of model.

2.2. Damage model (DM)

For a pure damage model, no inelastic strain is considered, and the damage variable is driven by the maximum previously reached strain level. This model fits into the general framework (6)–(7) if we set

$$f_d(\kappa_d, \varepsilon) = \varepsilon - \kappa_d \tag{8}$$

$$D = g_d(\kappa_d) \tag{9}$$

$$\varepsilon_p = 0 \tag{10}$$

Function g_d controls the shape of the local stress-strain curve and directly corresponds to the function previously denoted as g; see Eq. (4).

2.3. Damage-plastic model (DPM)

A popular family of damage-plastic models is based on a yield function written in terms of the effective stress and on damage driven by the cumulative plastic strain. Loading-unloading conditions corresponding to the plastic part of the model read

$$f_p(\ldots, \kappa_p) \le 0, \qquad \dot\kappa_p \ge 0, \qquad f_p(\ldots, \kappa_p)\,\dot\kappa_p = 0 \tag{11}$$

where f_p is the yield function, and κ_p is the cumulative plastic strain. In the present one-dimensional context with tensile yielding only, the yield function can be defined as

$$f_p(\tilde\sigma, \kappa_p) = \tilde\sigma - \sigma_Y(\kappa_p) \tag{12}$$

where (Lemaitre and Chaboche, 1985)

$$\tilde\sigma = \frac{\sigma}{1-D} = E(\varepsilon - \varepsilon_p) \tag{13}$$

is the effective stress and σ_Y is a function that describes the dependence of the current yield stress on the cumulative plastic strain (isotropic hardening).

In the present simple case (yielding under uniaxial tension), there is no difference between the plastic strain and the cumulative plastic strain, which is formally described by the rate equation

$$\dot\varepsilon_p = \dot\kappa_p \tag{14}$$

with the initial values of both ε_p and κ_p set to zero. The cumulative plastic strain at the same time plays the role of the damage-driving variable, and so we set

$$f_d(\kappa_d, \varepsilon_p) = \varepsilon_p - \kappa_d \tag{15}$$

$$D = g_{dp}(\kappa_d) \tag{16}$$

The shape of the stress-strain diagram is affected by functions σ_Y and g_{dp}.

2.4. Model with damage-driven inelastic strain (DMIS)

In contrast to the previous model with damage driven by plastic strain, here we use the opposite approach. A pure damage model with damage driven by the total strain is enhanced by inelastic strain that depends on the damage variable (Hermann and Kestin, 1988; Borderie, 1991; Halm and Dragon, 1998; Lebon, 2011). This is described by

$$f_d(\kappa_d, \varepsilon) = \varepsilon - \kappa_d \tag{17}$$

$$D = g_{dis}(\kappa_d) \tag{18}$$

$$\varepsilon_p = \alpha_{dis}(D) \tag{19}$$

The shape of the stress-strain diagram is affected by functions α_{dis} and g_{dis}.

2.5. Correspondence between local models

For a fair evaluation of the effects of nonlocality, we need to make sure that the local response of the considered models is the same, or at least similar. The pure damage model (DM) from Section 2.2 is used as the starting point, and the other two models from Sections 2.3–2.4 are adjusted (cross-identified) so that they give the same stress-strain curve under monotonic loading.

According to the **damage model (DM)** described by (6)–(10), we get

$$\sigma = \sigma_d(\varepsilon) \equiv [1 - g_d(\varepsilon)]E\varepsilon \tag{20}$$

For a given stress-strain diagram described by function σ_d, the corresponding damage function is easily evaluated as

$$g_d(\varepsilon) = 1 - \frac{\sigma_d(\varepsilon)}{E\varepsilon} \tag{21}$$

For the **damage-plastic model (DPM)** described by (6)-(7) and (11)–(16), we first have to evaluate the dependence of the plastic strain on the total strain by solving equation

$$E(\varepsilon - \varepsilon_p) = \sigma_Y(\varepsilon_p) \tag{22}$$

which can be derived by combining (12)–(14) with the assumption of plastic yielding, characterized by $f_p = 0$. Once ε_p is known as a function of ε, we can express from (13) the effective stress

$$\tilde\sigma(\varepsilon) = E[\varepsilon - \varepsilon_p(\varepsilon)] \tag{23}$$

and then, from (6) combined with (16), also the nominal stress

$$\begin{aligned}\sigma &= \sigma_{dp}(\varepsilon) \equiv [1 - g_{dp}(\varepsilon_p(\varepsilon))]\,\tilde\sigma(\varepsilon) \\ &= [1 - g_{dp}(\varepsilon_p(\varepsilon))]\,E\,[\varepsilon - \varepsilon_p(\varepsilon)]\end{aligned} \tag{24}$$

If function σ_{dp} describing the stress-strain diagram is known, the above equations are not sufficient to identify two independent functions of the damage-plastic model, g_{dp} and σ_Y. One can first select an arbitrary function σ_Y and then determine

$$g_{dp}(\varepsilon_p) = 1 - \frac{\sigma_d(\varepsilon_p + \sigma_Y(\varepsilon_p)/E)}{\sigma_Y(\varepsilon_p)} \tag{25}$$

Table 1
Three versions of the DMIS (and two subversions as special cases).

Version	Parameters	$g_{dis}(\varepsilon)$	$\alpha_{dis}(D)$
1	ε_0, ε_f, E_{ep}	$1-\dfrac{1}{1+(E_{ep}/E)(\varepsilon/\varepsilon_0-1)}\exp\left(-\dfrac{\varepsilon-\varepsilon_0}{\varepsilon_f-\varepsilon_0}\right)$	$g^*_{dis}(D)-\dfrac{\sigma_d(g^*_{dis}(D))}{E(1-D)}$
1s	ε_0, ε_f	$1-\exp\left(-\dfrac{\varepsilon-\varepsilon_0}{\varepsilon_f-\varepsilon_0}\right)$	$-(\varepsilon_f-\varepsilon_0)\ln(1-D)$
2	α, p	implicitly given by (75)	αD^p
2s	α	$\dfrac{\varepsilon+\alpha-\sqrt{(\varepsilon+\alpha)^2-4\alpha[\varepsilon-\sigma_d(\varepsilon)/E]}}{2\alpha}$	αD
3	α	$\dfrac{\varepsilon-\sigma_d(\varepsilon)/E}{\varepsilon+\alpha}$	$\dfrac{\alpha D}{1-D}$

In this way, it is possible to construct pairs of functions g_{dp} and σ_Y that correspond to exactly the same stress-strain curve under monotonic loading but to different unloading branches.

For the **damage model with inelastic strain (DMIS)** described by Eqs. (6)-(7) and (17)–(19), the stress under monotonic loading is expressed as

$$\sigma=\sigma_{dis}(\varepsilon)\equiv[1-g_{dis}(\varepsilon)]\,E\,[\varepsilon-\alpha_{dis}(g_{dis}(\varepsilon))] \tag{26}$$

Again, we have two functions to determine, g_{dis} and α_{dis}. Suppose that we want to match not only the monotonic stress-strain curve but also the unloading branches of the diagram that correspond to the damage-plastic model. These requirements lead to conditions of equal stress values and equal damage values generated by both models at each strain level:

$$[1-g_{dis}(\varepsilon)]\,E\,[\varepsilon-\alpha_{dis}(g_{dis}(\varepsilon))]=\sigma_d(\varepsilon) \tag{27}$$

$$g_{dis}(\varepsilon)=g_{dp}(\varepsilon_p(\varepsilon)) \tag{28}$$

The second condition gives directly function g_{dis}, and then from the first condition we get a formula for the composed function

$$\alpha_{dis}(g_{dis}(\varepsilon))=\varepsilon-\frac{\sigma_d(\varepsilon)}{E[1-g_{dis}(\varepsilon)]} \tag{29}$$

To construct an explicit formula for α_{dis}, we must invert g_{dis} and then set

$$\alpha_{dis}(D)=g^*_{dis}(D)-\frac{\sigma_d(g^*_{dis}(D))}{E(1-D)} \tag{30}$$

where g^*_{dis} denotes the inverse function of g_{dis}.

2.6. Example—Exponential softening

To provide a specific example, consider a stress-strain diagram with linear elasticity up to the peak, followed by exponential softening. Under monotonic loading, the dependence of stress on strain is described by

$$\sigma(\varepsilon)=\begin{cases}E\varepsilon & \text{for } \varepsilon\le\varepsilon_0\\ f_t\exp\left(-\dfrac{\varepsilon-\varepsilon_0}{\varepsilon_f-\varepsilon_0}\right) & \text{for } \varepsilon>\varepsilon_0\end{cases} \tag{31}$$

where f_t is the tensile strength, $\varepsilon_0=f_t/E$ is the limit elastic strain, and ε_f is a parameter that controls the steepness of the softening branch. This is the model that was used in one-dimensional examples in Desmorat et al. (2015).

For the **pure damage model (DM)**, we need to get $\sigma_d(\varepsilon)=\sigma(\varepsilon)$, and so the damage function has to be set to

$$g_d(\varepsilon)=1-\frac{\sigma(\varepsilon)}{E\varepsilon}=\begin{cases}0 & \text{for } \varepsilon\le\varepsilon_0\\ 1-\dfrac{\varepsilon_0}{\varepsilon}\exp\left(-\dfrac{\varepsilon-\varepsilon_0}{\varepsilon_f-\varepsilon_0}\right) & \text{for } \varepsilon>\varepsilon_0\end{cases} \tag{32}$$

as already indicated in (5), where the damage function was denoted simply as g.

Since the monotonic stress-strain law does not uniquely define the models with plastic or inelastic strains, we use an additional assumption that the **damage-plastic model (DPM)** is characterized by **linear hardening of its plastic part**. The dependence of the effective yield stress on plastic strain is thus given by

$$\sigma_Y(\varepsilon_p)=f_t+H\varepsilon_p \tag{33}$$

where f_t is the initial yield stress (playing also the role of tensile strength) and $H\ge 0$ is the hardening modulus. To get the same exponential softening law (31) as for the damage model, we need to define the damage function of the damage-plastic model according to (25) as

$$\begin{aligned}g_{dp}(\varepsilon_p)&=1-\frac{\sigma_d(\varepsilon_p+\sigma_Y(\varepsilon_p)/E)}{\sigma_Y(\varepsilon_p)}\\ &=1-\frac{f_t}{f_t+H\varepsilon_p}\exp\left(-\frac{(1+H/E)\varepsilon_p}{\varepsilon_f-\varepsilon_0}\right)\end{aligned} \tag{34}$$

For the linear hardening law (33), Eq. (22) has a linear form

$$E(\varepsilon-\varepsilon_p)=f_t+H\varepsilon_p \tag{35}$$

and can be solved analytically. The resulting dependence of plastic strain on total strain (during monotonic loading) is given by

$$\varepsilon_p(\varepsilon)=\frac{E\varepsilon-f_t}{E+H} \tag{36}$$

Now we can proceed to the **damage model with inelastic strain (DMIS)** and match it to the DPM model. Various versions of the DMIS model can be constructed, with the same monotonic stress-strain curve (exponential) but different rules for the slope of unloading branches. Three typical cases are analyzed in detail in Appendix A and summarized in Table 1.

Version 1 is constructed such that the local stress-strain curve (including unloading) exactly matches that obtained with the DP model. Parameter H of the DP model, which represents the plastic modulus, is transformed into the elastoplastic modulus

$$E_{ep}=\frac{EH}{E+H} \tag{37}$$

For a nonzero value of H, function g_{dis} cannot be inverted in closed form and the inverse function g^*_{dis} must be evaluated numerically. In the special case of $H=0$, which is in Table 1 referred to as version 1s, function g_{dis} gets simpler and its inversion can be done analytically, which leads to a closed-form expression for function α_{dis}.

Instead of matching the unloading response to the DP model, one can match only the response during monotonic loading and select the specific form of function α_{dis} as needed. If this function is postulated as a power law with a general exponent p, the corresponding function g_{dis} cannot be obtained in closed form and must be computed numerically; see version 2 in Table 1. In the special case with exponent $p=1$ (version 2s in Table 1), an analytical formula for g_{dis} can be derived. Also, for another simple form of α_{dis} given by $\alpha D/(1-D)$ (which goes to infinity when D tends to 1),

the corresponding function g_{dis} can be constructed; see version 3 in Table 1. A detailed analysis of the specific forms of functions g_{dis} and α_{dis} for individual versions of the model is provided in Appendix A.

2.7. Algorithmic treatment

For the pure damage model, the evaluation of damage and stress that correspond to a given strain increment is straightforward. For the damage-plastic model, it could be somewhat more involved in a general multiaxial case—one would need to first compute the effective stress and cumulative plastic strain using an elastoplastic stress-return algorithm and then evaluate the resulting damage and nominal stress (Grassl and Jirásek, 2006; Valentini and Hofstetter, 2013). However, in the present uniaxial case, the elastoplastic stress return algorithm can be replaced by simple rules that compare the elastically evaluated trial stress with the stress value that would correspond to the current total strain under monotonic loading.

More attention needs to be paid to the damage model with inelastic strain, which can be considered in several versions that differ by the rules for unloading; see Table 1. The stress evaluation algorithm for the DMIS can be summarized as follows:

1. First, the value of κ_d is determined by updating the maximum strain reached so far.
2. The next step depends on the particular version of the model.
   (a) **Version 1, including 1s:** Based on Eqs. (18) and (66), we compute damage and inelastic strain:

$$D = g_{dis}(\kappa_d) = 1 - \frac{1}{1+(E_{ep}/E)(\kappa_d/\varepsilon_0-1)} \exp\left(-\frac{\kappa_d-\varepsilon_0}{\varepsilon_f-\varepsilon_0}\right) \tag{38}$$

$$\varepsilon_p = \beta_{dis}(\kappa_d) = \frac{E}{E+H}(\kappa_d-\varepsilon_0) \tag{39}$$

   (b) **Version 2:** Based on Eq. (75), with $\sigma_d(\varepsilon)$ given by (31) and $\alpha_{dis}(D)$ by (78), we compute damage iteratively as the limit of D_k given by

$$D_k = D_{k-1} - \frac{F(D_{k-1})}{F'(D_{k-1})}, \qquad k = 1, 2, \dots \tag{40}$$

   starting from $D_0 = 0$ and checking that the iterated values remain between 0 and 1. Function F and its derivative F' are defined in (79)-(80). Then we evaluate

$$\varepsilon_p = \alpha_{dis}(D) \tag{41}$$

   (c) **Version 2s:** Based on Eqs. (71) and (73), with $\sigma_d(\kappa_d)$ given by (31), we compute damage and inelastic strain:

$$D = g_{dis}(\kappa_d) = \frac{\kappa_d+\alpha}{2\alpha} - \sqrt{\left(\frac{\kappa_d-\alpha}{2\alpha}\right)^2 + \frac{\varepsilon_0}{\alpha}\exp\left(-\frac{\varepsilon-\varepsilon_0}{\varepsilon_f-\varepsilon_0}\right)} \tag{42}$$

$$\varepsilon_p = \alpha_{dis}(D) = \alpha D \tag{43}$$

   (d) **Version 3:** Based on Eq. (74), with $\sigma_d(\varepsilon)$ given by (31) and $\alpha_{dis}(D)$ by (81), we compute damage and inelastic strain:

$$D = g_{dis}(\kappa_d) = \frac{\kappa_d - \sigma_d(\kappa_d)/E}{\kappa_d+\alpha} = \frac{\kappa_d}{\kappa_d+\alpha} - \frac{\varepsilon_0}{\kappa_d+\alpha}\exp\left(-\frac{\varepsilon-\varepsilon_0}{\varepsilon_f-\varepsilon_0}\right) \tag{44}$$

$$\varepsilon_p = \alpha_{dis}(D) = \alpha\frac{D}{1-D} \tag{45}$$

3. Finally, the stress is obtained as

$$\sigma = (1-D)E(\varepsilon-\varepsilon_p) \tag{46}$$

3. Nonlocal formulations

3.1. Fixed interaction distance

In general, nonlocal formulations of the models described in Sections 2.1–2.4 can be based on weighted spatial averaging of the damage-driving variable. The standard nonlocal approach would use a fixed weight function $\alpha(x, \xi)$, defined for instance as

$$\alpha(x,\xi) = \frac{\alpha_0(|x-\xi|)}{\int_{\mathcal{L}}\alpha_0(|x-\eta|)\,\mathrm{d}\eta}, \qquad r = |x-\xi| \tag{47}$$

where $\mathcal{L}$ is the one-dimensional domain of interest, usually taken as the interval $[0, L]$ where L is the length of the analyzed bar, and α_0 is a suitable function describing the decay of nonlocal interaction effects with increasing distance r. This function can be taken for instance as

$$\alpha_0(r) = \left\langle 1 - \left(\frac{r}{R}\right)^2\right\rangle^2 \tag{48}$$

where $\langle\dots\rangle$ are Macauley brackets (denoting the positive part, i.e., $\langle x\rangle = \max(0, x)$), and R is a model parameter with the dimension of length, which reflects the internal length scale of the material and is referred to as the nonlocal interaction radius. Physically, R should be related to the size and spacing of major heterogeneities in the material microstructure. Standard nonlocal models consider the interaction radius R as a fixed parameter. Since the growth of defects modifies the microstructure and affects mechanical interactions on the scale of heterogeneities, it is more realistic to treat the interaction distance as evolving, which motivates the modifications that will be introduced in Section 4.3.

For the pure damage model (DM), damage is driven by the maximum previously reached value of the equivalent strain, which, in the one-dimensional case, equals the total strain. In displacement-based versions of the finite element method, the strain at the end of an incremental computational step is iteratively updated, and in each iteration it is treated as a given quantity. Therefore, evaluation of the nonlocal strain

$$\bar{\varepsilon}(x) = \int_{\mathcal{L}}\alpha(x,\xi)\varepsilon(\xi)\,\mathrm{d}\xi \tag{49}$$

is fully explicit. The same holds for the DMIS. In nonlocal versions of these models (DM or DMIS), Eq. (8) or (17) is replaced by

$$f_d(\kappa_d, \bar{\varepsilon}) = \bar{\varepsilon} - \kappa_d \tag{50}$$

The stress evaluation algorithm remains the same, just the meaning of the damage-driving variable is different. If needed, one could also use an over-nonlocal formulation, with the loading function defined as

$$f_d(\kappa_d, \bar{\varepsilon}, \varepsilon) = m\bar{\varepsilon} + (1-m)\varepsilon - \kappa_d \tag{51}$$

where m is an additional dimensionless parameter. Values $m = 0$ and $m = 1$ would correspond to the local model and standard nonlocal model, respectively. The so-called over-nonlocal formulation uses $m > 1$. It was originally proposed for nonlocal plasticity (Vermeer and Brinkgreve, 1994; Strömberg and Ristinmaa, 1996), and later adapted to nonlocal plasticity combined with damage (Grassl and Jirásek, 2006), but it is in principle applicable to damage with inelastic strain as well.

For the damage-plastic model, the damage-driving variable is the maximum previously reached value of the cumulative plastic strain. In the nonlocal version and one-dimensional setting, Eq. (15) is replaced by

$$f_d(\kappa_d, \bar{\varepsilon}_p) = \bar{\varepsilon}_p - \kappa_d \tag{52}$$

where

$$\bar{\varepsilon}_p(x) = \int_{\mathcal{L}} \alpha(x,\xi)\varepsilon_p(\xi)\,\mathrm{d}\xi \tag{53}$$

is the nonlocal plastic strain. In a general multiaxial setting, the nonlocal cumulative plastic strain would be used. Again, one can envision an over-nonlocal formulation (Grassl and Jirásek, 2006), with

$$f_d(\kappa_d, \bar{\varepsilon}_p, \varepsilon_p) = m\bar{\varepsilon}_p + (1-m)\varepsilon_p - \kappa_d \tag{54}$$

3.2. Damage-dependent interaction distance

The nonlocal formulations described in the previous subsection consider the nonlocal weight function $\alpha_0(r)$ as fixed. The strength of nonlocal interaction decays with increasing distance r between points x and ξ.

As mentioned in the Introduction, a constant internal length (here the nonlocal interaction radius R) associated with the standard definition $r = |x-\xi|$ of the interaction distance between points x and ξ provides regularization and removes pathological sensitivity to the mesh, but also leads to a spurious expansion of the damage profile at late stages of the failure process (Bažant and Pijaudier-Cabot, 1988). This is due to the fact that, in the averaging of the damage-driving variable, points located on the opposite sides of a highly damaged zone interact in the same manner as in the zero- or low-damage case. A new form of nonlocal integral averaging that makes a highly damaged zone (at $D \approx 1$) equivalent to a crack has been proposed in Desmorat and Gatuingt (2007, 2010) and Desmorat et al. (2010), following the idea that elastic wave propagation is slowed down by a damage field, possibly heterogeneous, in a so-called nonlocal integral formulation with an internal time instead of an internal length (see also Rojas-Solano et al., 2013, in which the non-local interactions are computed by means of thermal expansions of circular inclusions centered at each material point).

Analogy with formulations based on internal time motivates nonlocal models with interaction distance modified by damage. In 1D, the effective distance $\tilde{r}$ between points x and ξ is defined in (1), for easier reference rewritten here:

$$\tilde{r}(x,\xi) = \int_{\min(x,\xi)}^{\max(x,\xi)} \frac{\mathrm{d}\eta}{\sqrt{1-D(\eta)}} \tag{55}$$

The effective distance is then used for evaluation of the modified nonlocal weight function

$$\alpha(x,\xi) = \frac{\alpha_0(\tilde{r}(x,\xi))}{\int_{\mathcal{L}} \alpha_0(\tilde{r}(x,\eta))\,\mathrm{d}\eta} \tag{56}$$

Evaluation of the effective distance is greatly facilitated by the fact that, in the one-dimensional space, points x and ξ are connected by one single path (straight segment) and the effective distance is obtained simply by summing the effective lengths of all infinitesimal segments into which this path is divided. In multiple dimensions, a straight path does not always lead to the shortest effective distance, and minimization over all possible continuous paths connecting x with ξ needs to be invoked (Desmorat et al., 2015): the effective distances are computed in a Riemannian space curved by damage (see (Rastiello et al., 2018) for 2D computations using Fast Marching methods). The associated (general) computational procedures are not studied in the present work. Here we focus on fundamental localization properties of models with damage-dependent nonlocal interaction (55), which can be assessed in one spatial dimension.

3.3. Evaluation of effective distance by numerical integration

In numerical simulations by finite elements, the integral in (55) must be approximated by a finite sum, and it is natural and convenient to use the same set of Gauss integration points that are used for the evaluation of internal forces and stiffness coefficients. Typically, linear two-node elements with one integration point per element are used.

Suppose that the Gauss points are numbered consecutively and arranged in ascending order according to their x-coordinate. In a straightforward implementation, the numerical evaluation of the effective distance between points x_i and x_j (with $j > i$) can be based on the trapezoidal rule, which leads to

$$\begin{aligned}\tilde{r}(x_i,x_j) &= \int_{x_i}^{x_j} \frac{\mathrm{d}x}{\sqrt{1-D(x)}} \\ &\approx \sum_{k=i+1}^{j} \frac{1}{2}\left(\frac{1}{\sqrt{1-D(x_{k-1})}} + \frac{1}{\sqrt{1-D(x_k)}}\right)(x_k - x_{k-1})\end{aligned} \tag{57}$$

This rule would be exact if the function $1/\sqrt{1-D(x)}$ were linear between the neighboring Gauss points. However, if D approaches 1 at the center of the damage zone, function $1/\sqrt{1-D(x)}$ becomes highly nonlinear and the integration error increases. Numerical results show that the distribution of damage between neighboring Gauss points is close to linear, and so it is better to approximate $D(x)$ by a linear function and perform an analytical integration. The contribution of one typical subinterval is then evaluated as

$$\begin{aligned}\int_{x_{k-1}}^{x_k} \frac{\mathrm{d}x}{\sqrt{1-D(x)}} &\approx \int_{x_{k-1}}^{x_k} \frac{\mathrm{d}x}{\sqrt{1-D(x_{k-1})\frac{x_k-x}{x_k-x_{k-1}} - D(x_k)\frac{x-x_{k-1}}{x_k-x_{k-1}}}} \\ &= \frac{2(x_k-x_{k-1})}{\sqrt{1-D(x_{k-1})}+\sqrt{1-D(x_k)}}\end{aligned} \tag{58}$$

and the resulting modified distance is given by

$$\tilde{r}(x_i,x_j) = 2\sum_{k=i+1}^{j} \frac{x_k - x_{k-1}}{\sqrt{1-D(x_{k-1})}+\sqrt{1-D(x_k)}} \tag{59}$$

In the next section, it will be demonstrated that numerical results obtained with this improved integration scheme are better, not only for the pure damage model (Fig. 1a), but also for the damage-plastic model (Fig. 3) and for the damage model with inelastic strain (Fig. 6).

4. Numerical results for models with exponential softening

4.1. Setup of the uniaxial localization test

Localization properties of nonlocal versions of the constitutive models DM, DPM and DMIS described in Section 2 will be studied via simulations of a prismatic bar fixed at its left end and subjected to an increasing displacement imposed at its right end. Body forces, inertia effects and rate dependence of the material response are neglected, which means that the equilibrium condition is reduced to the condition of uniform stress along the bar. The bar length is set to $L = 100$ mm and the sectional area is supposed to be constant along the bar (its precise value is irrelevant because all the results will be presented in terms of stresses instead of forces). The material is characterized by Young's modulus $E = 30$ GPa and uniaxial tensile strength $f_t = 3$ MPa, which corresponds to the limit elastic strain $\varepsilon_0 = f_t/E = 10^{-4}$. The local stress-strain curve under monotonic loading is supposed to be given by (31), with $\varepsilon_f = 10^{-3}$. Objectivity of the model and finite energy dissipation are enforced by a nonlocal formulation. The bell-shaped polynomial weight function (48) is used, with the radius of nonlocal interaction set to $R = 20$ mm.

The present study is focused on the evolution of the damage zone inside the specimen and on the global post-peak response. The meshes are graded such that the spatial resolution in

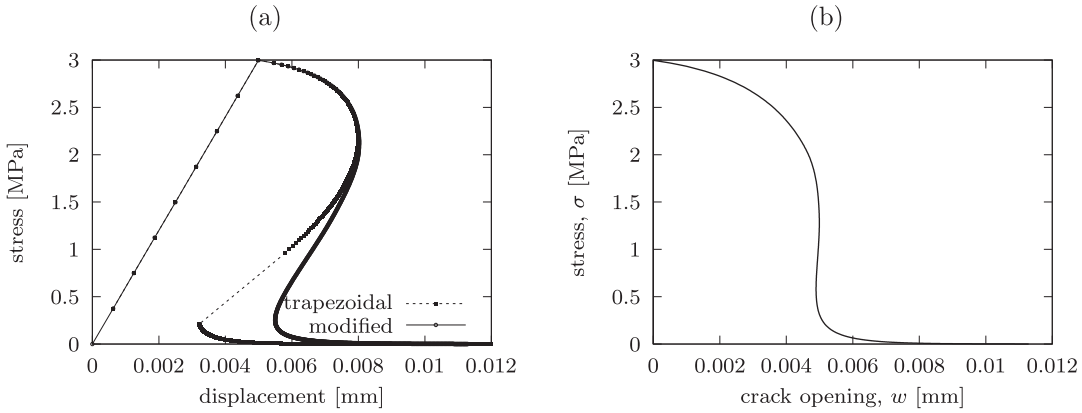

Fig. 1. (a) Influence of the integration scheme on stress-displacement diagrams for nonlocal damage model with damage-dependent nonlocal interaction: "trapezoidal" = effective distance evaluated using (57), "modified" = effective distance evaluated using (59), (b) cohesive curve extracted by subtracting the elastic elongation.

the expected damage zone near the middle section is sufficient. The number of elements is always odd and the axis of symmetry passes through the center of an element (not through a node of the finite element mesh). Localization is triggered by the reduction of the sectional area of the central element by 0.1%. The mesh referred to as "coarse" consists of 45 elements and the element size in the damage zone is equal to 2 mm. The mesh referred to as "medium" consists of 121 elements and the element size in the damage zone is equal to 0.95 mm. The mesh referred to as "fine" consists of 241 elements and the element size in the damage zone is equal to 0.49 mm.

Even though the weakened element is located in the middle of the bar and damage is first initiated in this element, the subsequent evolution of the numerically resolved damage zone may lead to a loss of symmetry, due to round-off error. In computations on very fine meshes, the damage process is sometimes attracted by one of the boundaries. The effect of a boundary on the nonlocal averaging operator is a separate issue, not treated in the present study. Since we deliberately restrict attention to localized solutions unaffected by the boundary, it is desirable to keep the center of the process zone in the middle of the bar. This could be achieved by using a more dramatic weakening of the central element. In the present context, it is preferable to keep the imposed imperfection as small as possible, in order to reduce its effect on the final stages of localization, when damage grows in only a few elements around the weakened one.

It turns out that potential localization at the boundary can be efficiently suppressed by imposing symmetry of the solution with respect to the middle section of the bar (because then the damage zone cannot localize at one boundary only but it would have to localize at both, which is energetically less favorable). In the numerical model, symmetry is enforced by treating the nodal displacements in the left half of the bar as primary unknowns and the nodal displacements in the right half of the bar as dependent quantities (symmetrically mirrored), using the master-slave concept. Of course, the boundary conditions need to be adjusted in the sense that one half of the bar elongation is applied on the left boundary in the negative direction and the other half on the right boundary in the positive direction. To capture potential snapbacks in a stable way, the simulation is run under indirect displacement control, with the elongation of the weakest element used as a monotonically increasing control variable.

4.2. Damage model (DM)

For the pure damage model with exponential softening, one-dimensional simulations of strain localization were performed in Desmorat et al. (2015), with the conclusion that the global response of the bar becomes increasingly brittle at later stages of the localization process. The computed load-displacement diagrams (here actually stress-displacement diagrams) exhibit a dramatic snapback. To capture this behavior in a stable way, the simulation is performed under indirect displacement control, with the control variable defined as the relative displacement of the nodes of the element crossing the axis of symmetry. Equivalently, one could describe the loading process as being controlled by the maximum local strain.

Despite the careful choice of the control variable, it turns out that a simulation with evaluation of the effective interaction distance based on the trapezoidal rule (57) leads to a solution which does not evolve in a continuous fashion until complete failure of the specimen. At a certain stage of the degradation process, the numerical solution (stress and total elongation of the bar) changes by a jump within one incremental step, even if the step size is prescribed as very small (see the dashed curve in Fig. 1a). This jump in global response is accompanied by a sudden localization of damage increments into one single element (while before the jump the zone of growing damage spans over five or more elements). The dashed curve plotted in Fig. 1 has been obtained for the coarse mesh but the same problem arises even for finer meshes.

A careful examination of the numerical solution reveals that the problem originates from a poor performance of the trapezoidal rule applied to the integral in (57). If the integral is evaluated using formula (59), which is better adapted to the highly nonlinear character of the integrated function for damage values close to 1, then the simulations lead to a continuous response; see the solid curve in Fig. 1a. However, the diagram still exhibits snapback and the behavior at late stages of localization can be characterized as extremely brittle. This might be realistic for certain materials, but not for quasibrittle materials such as concrete, which are typically characterized by load-displacement diagrams with an initially steep descent followed by a long tail. Of course, if the quasibrittle specimen is large, the load-displacement diagram may exhibit snapback, but this would happen just after the peak and the softening part of the diagram would be convex.

Since the shape of the load-displacement diagram for a bar under tension is strongly affected by the bar length, it is useful to subtract the contribution of the elastic deformation from the total bar elongation and present the softening curve as the relation between stress and the inelastic part of elongation, which can be interpreted as the opening of an equivalent fictitious (cohesive) crack. For the numerical results obtained with the nonlocal damage model using the modified integration scheme, this is done in Fig. 1b. For each stress level between 0 and $f_t = 3$ MPa, the inelas-

tic elongation (i.e., the equivalent cohesive crack opening) is evaluated as the difference between the displacements in the post-peak part and in the pre-peak part of the complete diagram. In the pre-peak part, the response is exclusively elastic and the corresponding displacement is easily expressed as $u_{el} = L\sigma/E$. The resulting diagram in Fig. 1b is characterized by a gradual descent in the initial part, followed by a dramatic drop to almost zero stress at nearly constant crack opening. Such shape of softening curve is substantially different from cohesive diagrams that are used in concrete modeling (either directly as the law characterizing a fictitious crack model, or after transformation to inelastic strain as one ingredient of a smeared crack model).

In the literature, various types of cohesive diagrams for concrete, masonry and rock have been recommended, but none of them has a concave shape. The simplest one is a linear softening diagram, which often leads to relatively poor fits of experimental data. The agreement can be improved by using convex softening diagrams of the bilinear or exponential type. The optimal shape of the diagram for concrete was studied in detail by Hordijk (1991), who suggested to use a rather complicated relation

$$\frac{\sigma}{f_t} = \left(1 + \left(\frac{c_1 w}{w_c}\right)^3\right) \exp\left(-\frac{c_2 w}{w_c}\right) - \frac{w}{w_c}\left(1 + c_1^3\right) \exp(-c_2) \quad (60)$$

where w_c is the critical crack opening at which the stress vanishes, and c_1 and c_2 are additional dimensionless parameters that control the shape of the curve.

Convexity of softening curves for concrete has been confirmed by many experiments. In principle, the softening curve can be directly extracted from tension tests (Gopalaratnam and Shah, 1985; Lee et al., 2008), which are rather scarce for concrete, because they are not so easy to perform in a stable way in the post-peak range. An alternative procedure is to identify the optimal softening curve by inverse analysis of other tests that lead to tensile failure, e.g., of bending or wedge-splitting tests. To provide an example, Fig. 2b shows data obtained from three-point bending tests on notched concrete beams reported in Chen and Su (2013). The figure contains the characteristics of several different types of concrete with compressive strength ranging from 40 to 90 MPa. To facilitate the comparison, stresses on the vertical axis are normalized by the tensile strength and crack openings on the horizontal axis by the critical crack opening for each particular concrete. The solid curve in Fig. 2b corresponds to the Hordijk law (60) with $c_1 = 3$ and $c_2 = 6.93$. It is clear that the overall shape with initial steep softening followed by a longer tail is quite universal and is properly captured by the Hordijk formula. Of course, the fit could further be improved by adjusting the optimal values of parameters c_1 and c_2 for each concrete type separately.

Using the analytically described cohesive curve with $c_1 = 3$ and $c_2 = 6.93$ as an example for demonstration purposes, it is now possible to show how the load-displacement curve under uniaxial tension would be affected by the bar length. Consider the same material properties as in the previous computations, i.e., $f_t = 3$ MPa and $E = 30$ GPa, and let us set the critical crack opening to $w_c = 200$ μm, which is a typical value. For each value of crack opening w between 0 and w_c, it is easy to evaluate the corresponding stress σ from (60) and then calculate the total elongation of a bar of length L as $u = w + L\sigma/E$. In this way, the softening branch of the diagram is constructed, while the initial elastic branch is described simply by $u = L\sigma/E$. The resulting diagrams for bar length L set respectively to 100 mm, 400 mm and 800 mm are shown in Fig. 2a. For a very short bar, the contribution of elastic deformation is relatively small and the post-peak part of the diagram is similar to the initial cohesive curve, just rescaled from the normalized variables to the physical variables. For longer bars, the elastic compliance plays a more important role and unloading of long bar segments around the process zone may lead to a softening branch with snapback. As already mentioned, this snapback occurs at an early stage of softening and the shape of the softening branch remains convex.

The foregoing discussion shows that the global response of a bar simulated by the nonlocal damage model with damage-dependent interactions, characterized by the load-displacement curve in Fig. 1a, is not realistic for quasibrittle materials such as concrete. It is therefore interesting to check whether a more realistic shape of the softening branch could be obtained for damage models that combine stiffness degradation with irreversible strains, in the form of either a damage-plastic formulation, or a damage model with inelastic strain. Modification of the function used in the damage law could be an alternative remedy, to be examined later in Section 5 and in Appendix C.

4.3. Damage-plastic model (DPM)

As the starting point, we consider a formulation based on the plastic model with linear plastic hardening described by (33), for which the dependence of plastic strain on total strain (during monotonic loading) is given by (36). The softening curve is considered as exponential, which leads to function g_{dp} defined by (34).

Localization behavior of the nonlocal version of the damage-plastic model depends on the choice of the plastic modulus H. In Grassl and Jirásek (2006) it was shown that, in the context of a standard nonlocal formulation, $H = 0$ leads to a fully localized plastic zone. This is similar to the so-called basic nonlocal plastic model, which was analyzed, e.g., in Jirásek and Rolshoven (2003).

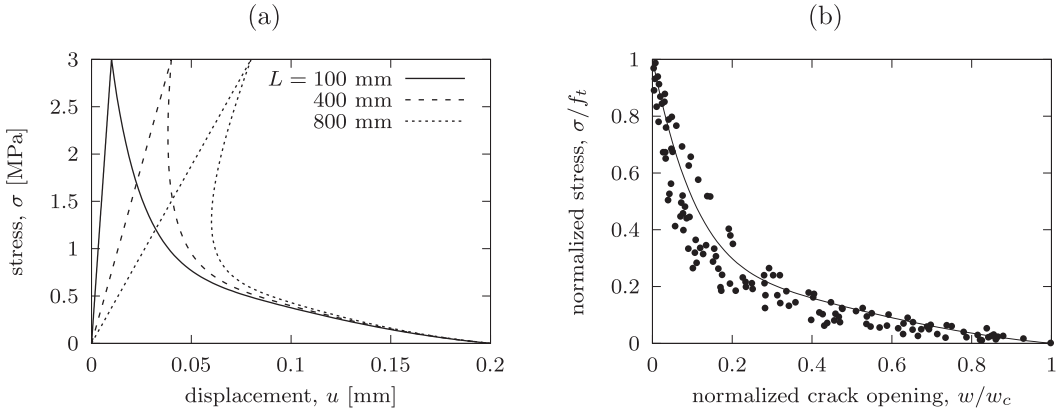

Fig. 2. (a) Normalized load-displacement diagrams for concrete bars of length 100 mm, 400 mm and 800 mm, (b) normalized plot of experimentally determined cohesive curves from Chen and Su (2013) and their fit by formula (60).

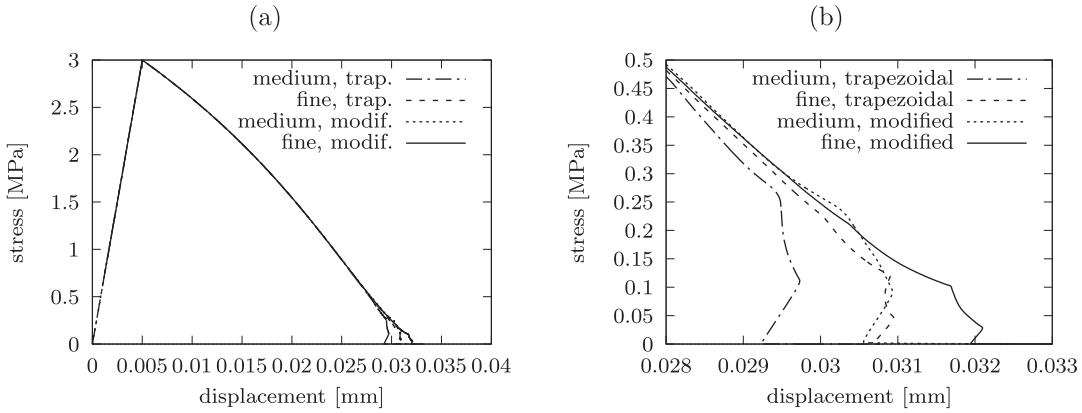

Fig. 3. Influence of the element size and integration scheme on stress-displacement diagrams for DPM with parameters $H = E/30$ and $m = 2$.

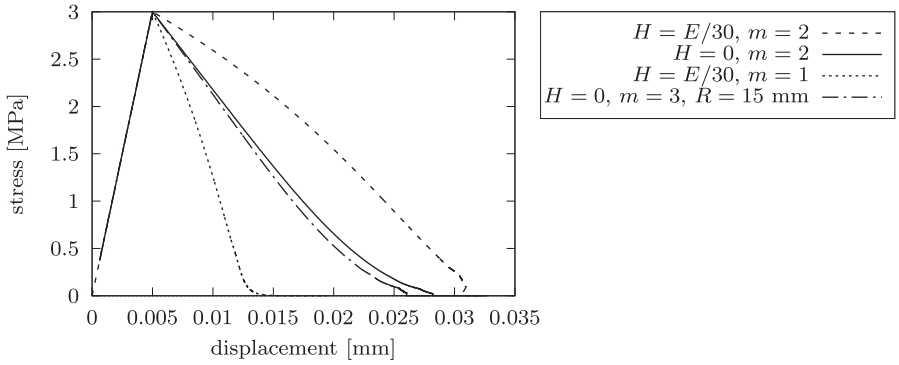

Fig. 4. Stress-displacement diagrams for DPM with various combinations of parameters.

In numerical simulations, the local plastic strain always localizes into one finite element, but the dissipation tends to a nonzero limit as the mesh is refined. The nonlocal plastic strain is nonzero in an interval of length $2R$ where R is the nonlocal interaction radius. Since the nonlocal plastic strain is the variable that drives damage, the damage variable is also nonzero in this interval. A finite size of the plastic zone is obtained if the plastic modulus H is set to a positive value, or if the damage is considered to be driven, according to (54), by the over-nonlocal plastic strain $m\bar{\varepsilon}_p + (1-m)\varepsilon_p$ with $m > 1$, or if both modifications are combined ($H > 0$ and $m > 1$).

The first simulation is performed with $H = E/30 = 1$ GPa and $m = 2$. All other parameters have the same values as in the previous case of a pure damage model, presented in Section 4.2. Nonlocal interaction weights are computed using the damage-dependent effective distance (55). The resulting stress-displacement curve plotted in Fig. 3a has a slightly concave shape and, in contrast to the curve obtained with the pure damage model (Fig. 1), does not exhibit a dramatic snapback. A closer examination of the terminal part of the curve reveals a slight snapback at a stage very close to complete failure, i.e., at a very low stress; see the close-up in Fig. 3b. The active part of the plastic zone gradually shrinks and the snapback occurs when the plastic strain increments become concentrated into one single element. This phenomenon is reduced if the mesh is refined, and also if the damage-dependent effective distance is evaluated using the modified scheme (59) instead of the trapezoidal rule (57). The quality of results obtained with the modified rule on the medium mesh is comparable to those obtained with the trapezoidal rule on the fine mesh. As the mesh is refined, the results seem to converge to a reasonable limit curve which has no snapback.

Fig. 4 shows how the shape of the stress-displacement curve is affected by model parameters. For reference, the results obtained with $H = E/30$ and $m = 2$ are shown as the dashed curve. The solid curve corresponds to an over-nonlocal model without hardening ($H = 0$ and $m = 2$); it has a slightly convex shape with a short tail. The dotted curve corresponds to a nonlocal (not over-nonlocal) model with hardening ($m = 1$, $H = E/30$). The shape is slightly concave, quite close to a straight line. Reduction of parameter m leads to a more brittle response, with reduced area under the stress-displacement curve. On the other hand, increasing m to 3 would lead to a wider damage profile and lower post-peak slope of the stress-displacement curve. We can compensate for that by reducing the nonlocal interaction radius R. The dash-dotted curve in Fig. 4 corresponds to an over-nonlocal formulation with $m = 3$, no hardening of the underlying plastic model ($H = 0$) and nonlocal interaction radius set to $R = 0.015$ m instead of the value $R = 0.02$ m, used in all the other simulations. The resulting shape of the stress-displacement diagram is very similar to that obtained for $m = 2$ and $R = 0.02$ m (solid curve).

As shown in Fig. 5a, the intermediate damage profiles obtained with $H = 0$ have a flat central part, but the final damage profile is nicely localized and damage tends to 1 at one section only. The flat central part of the damage profile is a characteristic feature of nonlocal damage-plastic models with no plastic hardening, as already observed in Grassl and Jirásek (2006). The zone of uniform damage corresponds to the active plastic zone, i.e., to the interval in which the local plastic strain is growing. In this interval, the yield condition is satisfied and, since the stress must be uniform along the whole bar (due to equilibrium), the product of the effective yield stress and the integrity factor $1 - D$ must be uniform along the active part of the plastic zone. For the formulation with a perfectly plastic model ($H = 0$) extended by damage, the effective yield stress remains equal to f_t, which leads to a uniform distribution of damage along the active part of the plastic zone. Damage is driven by the nonlocal plastic strain, and so the zone of growing damage is larger than the plastic zone, due to the

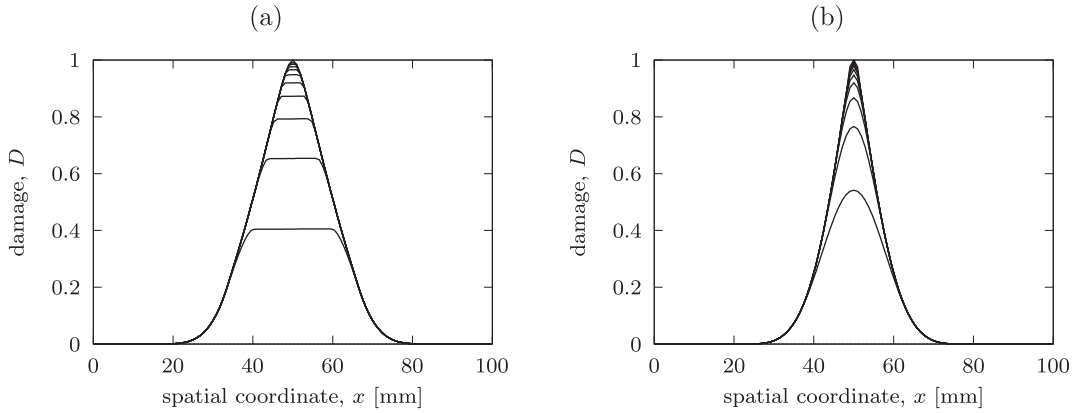

Fig. 5. Evolution of the damage profiles for DPM with parameters (a) $H = 0$ and $m = 2$, (b) $H = E/30$ and $m = 1$.

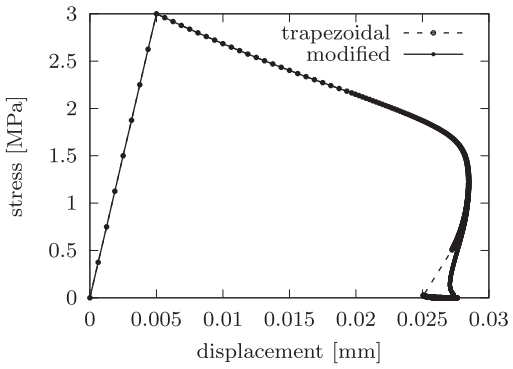

Fig. 6. Influence of the integration scheme on stress-displacement diagrams for DMIS (version 2, $\alpha = 10^{-3}$, $p = 0.8$).

effect of nonlocal averaging. However, both zones gradually shrink and damage tends to 1 exclusively in the central cross section. A more usual shape of the damage profiles is obtained for nonlocal damage-plastic models with a positive plastic modulus ($H > 0$), irrespective of whether the formulation is standard nonlocal ($m = 1$) or over-nonlocal ($m > 1$); see Fig. 5b.

The results are encouraging—the damage-plastic model with damage-dependent nonlocal interaction provides stress-displacement curves that do not exhibit a dramatic snapback and, for the over-nonlocal damage formulation combined with a perfectly plastic backbone model, the curves can even have a slightly convex shape with a short tail, while the active part of the damage zone gradually shrinks (which would not be the case for a nonlocal damage-plastic model with fixed interaction weights).

4.4. Damage model with inelastic strain (DMIS)

Let us now check whether a similar improvement of the shape of load-displacement diagrams can be achieved if the damage model is enriched by inelastic strain, as described in Section 2.4. Same as for the previously discussed models (DM and DPM), the modified integration scheme based on (59) leads to better results than the trapezoidal rule (57); see an example in Fig. 6, computed for version 2 of DMIS. Therefore, all subsequently reported results are computed using the modified scheme.

For versions 1 and 2 of the model, the stress-displacement diagrams exhibit snapback; see Fig. 7. Version 1 would give in the local 1D setting exactly the same response as the damage-plastic model introduced in Section 2.3. However, the nonlocal formulation leads to a different behavior, because the damage-plastic model evaluates damage from the nonlocal plastic strain while the DMIS evaluates plastic strain as well as damage from the nonlocal total strain. The solid curve in Fig. 7a corresponds to version 1 of DMIS derived from a damage-plastic model with no plastic hardening ($H = 0$), and the dashed curve to the DMIS derived from a damage-plastic model with linear plastic hardening ($H = E/30$). The response is continuous (thanks to the modified integration scheme) but the shape of the curves is similar to those obtained with the pure damage model, just the snapback occurs later.

The overall shape of the curve remains the same even for version 2s with inelastic strain proportional to damage; see the dashed curve in Fig. 7b. If the dependence of inelastic strain on damage is described by the power law (78), i.e., $\varepsilon_p = \alpha D^p$, with exponent p higher or smaller than 1, the shape is still the same;

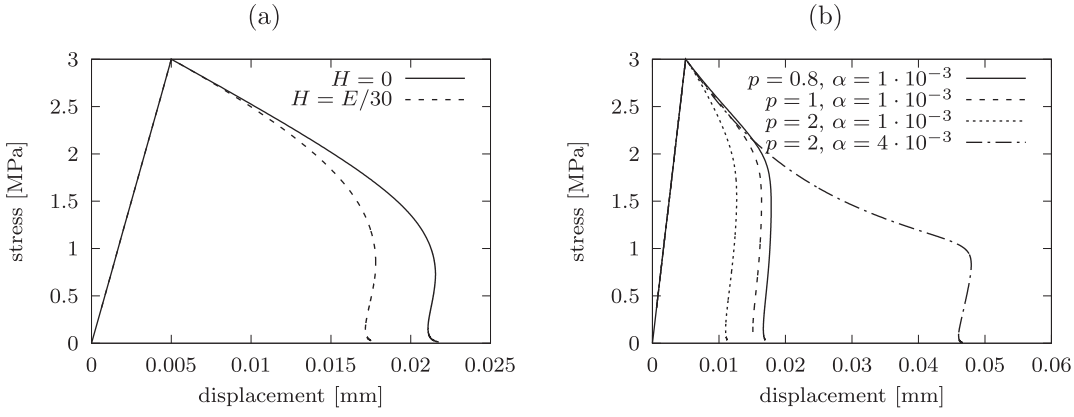

Fig. 7. Stress-displacement diagrams for DMIS: (a) version 1, (b) version 2.

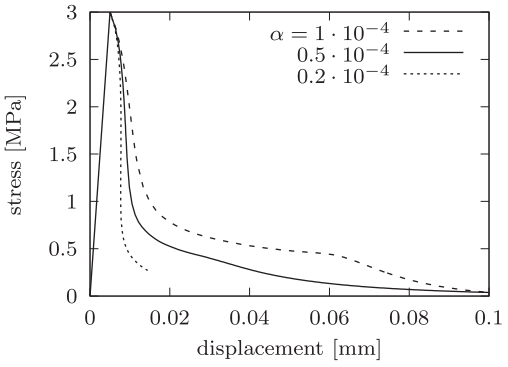

Fig. 8. Stress-displacement diagrams for version 3 of DMIS.

see the dotted and solid curves in Fig. 7b. An increase of parameter α only extends the ductile part of the curve and shifts the snapback to a later stage; see the dash-dotted curve.

Interestingly, quite an acceptable shape of the stress-displacement diagram is obtained with version 3 of the DPS model, which uses the hyperbolic law (45). Fig. 8 shows the diagrams obtained with various values of parameter α. The curves have a steep initial part followed by a very long tail. The tail is even somewhat too long, especially for the dashed curve that corresponds to $\alpha = 10^{-4}$. A reasonable load-displacement diagram was obtained with $\alpha = 0.5 \cdot 10^{-4}$; see the solid curve.

The evolution of damage, strain and plastic strain in the simulation with $\alpha = 0.5 \cdot 10^{-4}$ is plotted in Fig. 9. Plastic strains are localized in a narrow band (Fig. 9d) while damage is more spread out (Fig. 9a). In reality, the band in which plastic strain is nonzero coincides with the band in which damage is nonzero, but the plastic strain values that correspond to moderate damage levels are very small. For instance, for $D = 0.5$ the corresponding plastic strain is equal to α, which is only $0.05 \cdot 10^{-3}$ and on the scale of Fig. 9d such strains appear to be negligible. Plastic strains exceeding $0.5 \cdot 10^{-3}$ are attained only at points where damage exceeds 10/11. The final shape of the damage profile seems to be rounded but the band in which damage grows at late stages of the process is extremely narrow and eventually shrinks to one single integration point; see Fig. 9b (in this graph, values computed at Gauss integration points are connected by straight lines).

5. Damage-plastic model with double-exponential law

So far the most promising results, presented in Section 4.3, have been obtained with the damage-plastic model and parameters $H = 0$ and $m = 2$. However, the tail of the dashed stress-displacement curve in Fig. 4 may still be considered as too short for concrete; see e.g. Gopalaratnam and Shah (1985). For $H = 0$, the damage function (34) has the form

$$g_{dp}(\varepsilon_p) = 1 - \exp(-a\varepsilon_p) \tag{61}$$

where $a = 1/(\varepsilon_f - \varepsilon_0)$, and this type of law leads to an exponential shape of the local stress-strain diagram. To extend the tail, one can first try out a modified damage function that combines two exponentials:

$$g_{dp}(\varepsilon_p) = 1 - (1 - c_2)\exp(-a\varepsilon_p) - c_2 \exp(-a_2\varepsilon_p) \tag{62}$$

Here, c_2 and a_2 are two additional parameters. For $c_2 = 0$, the standard exponential law (61) is recovered. Parameters a and a_2 should be sufficiently different, just like relaxation times in viscoelasticity. The stress-displacement diagrams obtained with parameters $H = 0$ and $m = 2$ and with two sets of parameters of the double-exponential law (62) are shown in Fig. 10. The dashed curve corresponds to $a = 1000$, $a_2 = 100$ and $c_2 = 0.1$, and the solid curve to $a = 1200$, $a_2 = 120$ and $c_2 = 0.2$. For the second set of parameters, the stress-displacement curve has a very reasonable shape for concrete. The profiles of damage, plastic strain and nonlocal plastic strain obtained with these parameters are shown in Fig. 11. The

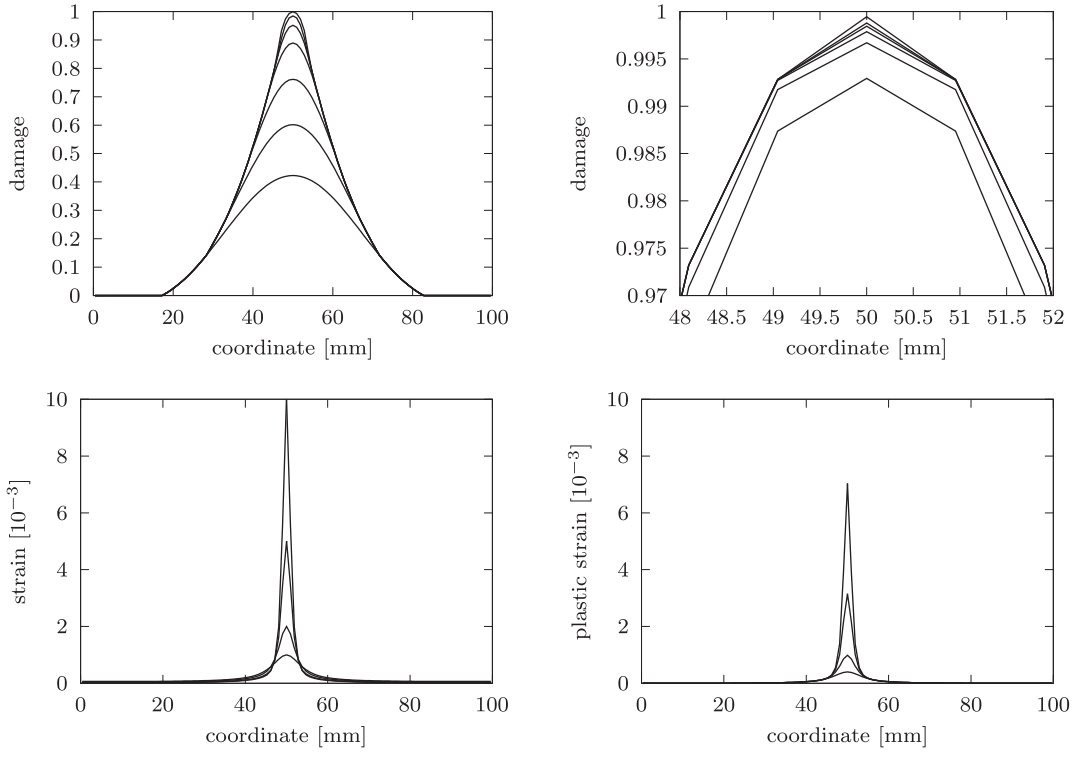

Fig. 9. Version 3 of DMIS with $\alpha = 0.5 \cdot 10^{-4}$: evolution of the profiles of (a)–(b) damage, (c) total strain, (d) plastic strain.

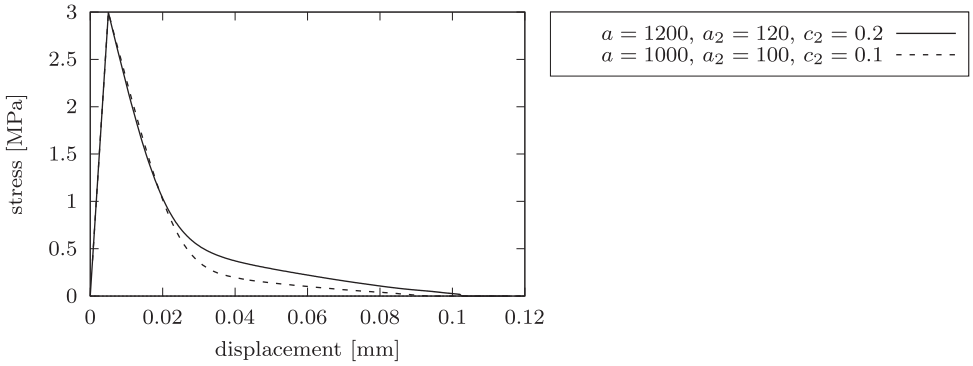

Fig. 10. Stress-displacement diagrams for DPM with double-exponential law (62) and parameters $H = 0$, $m = 2$.

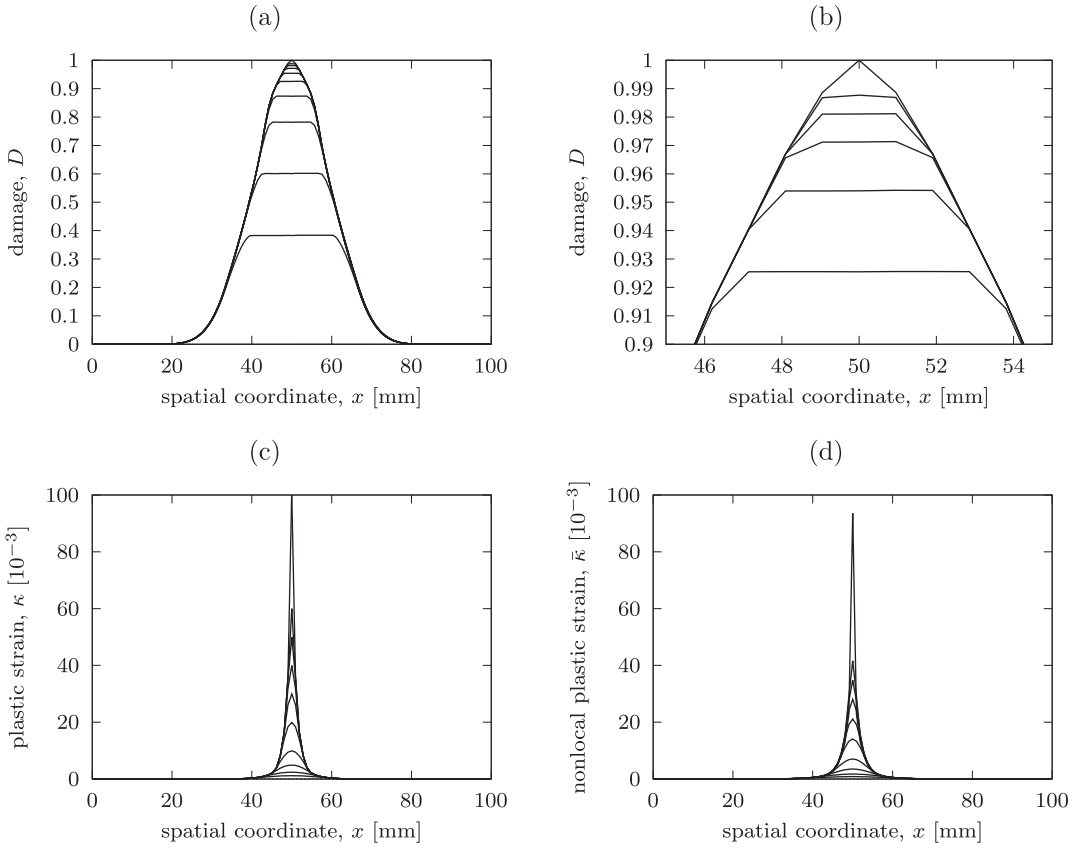

Fig. 11. Evolution of the profiles of (a)–(b) damage, (c) local plastic strain and (d) nonlocal plastic strain for DPM with double-exponential law (62) and parameters $H = 0$, $m = 2$.

damage profiles in Fig. 11a have a flat central part, for reasons explained in Section 4.3. The size of the active damage zone gradually decreases and damage tends to 1 at the central section only, as shown in Fig. 11b. The profiles of local and nonlocal plastic strain have the usual shape and are much more localized than the damage profiles; see Fig. 11c-d. On the scale of these graphs, the total strain profiles would look very similar to the (local) plastic strain profiles.

Since the approach based on the double-exponential softening law turns out to be successful for the damage-plastic model with no plastic hardening, we can also check its extension to the damage-plastic model with a positive hardening modulus H. If we used directly (62) for the damage-plastic model with $H > 0$, the resulting curve would exhibit non-physical bumps; see the dashed and dotted curves in Fig. 12a. Therefore, we need to be more careful.

The objective is to obtain a local softening curve described by the double-exponential function:

$$\sigma_d(\varepsilon) = f_t \left[(1 - c_2) \exp\left(-\frac{\varepsilon - \varepsilon_0}{\varepsilon_f - \varepsilon_0} \right) + c_2 \exp\left(-\frac{\varepsilon - \varepsilon_0}{\varepsilon_{f2} - \varepsilon_0} \right) \right] \tag{63}$$

For the damage-plastic model, this is achieved with

$$\begin{aligned} g_{dp}(\varepsilon_p) &= 1 - \frac{\sigma_d(\varepsilon_p + \sigma_Y(\varepsilon_p)/E)}{\sigma_Y(\varepsilon_p)} \\ &= 1 - \frac{f_t}{f_t + H\varepsilon_p} \left[(1 - c_2) \exp\left(-\frac{(1 + H/E)\varepsilon_p}{\varepsilon_f - \varepsilon_0} \right) \right. \\ &\qquad \left. + c_2 \exp\left(-\frac{(1 + H/E)\varepsilon_p}{\varepsilon_{f2} - \varepsilon_0} \right) \right] \end{aligned} \tag{64}$$

For $H = 0$, formula (64) reduces to (62) with $a = 1/(\varepsilon_f - \varepsilon_0)$ and $a_2 = 1/(\varepsilon_{f2} - \varepsilon_0)$, which means that $\varepsilon_f = \varepsilon_0 + 1/a$ and $\varepsilon_{f2} = \varepsilon_0 +$

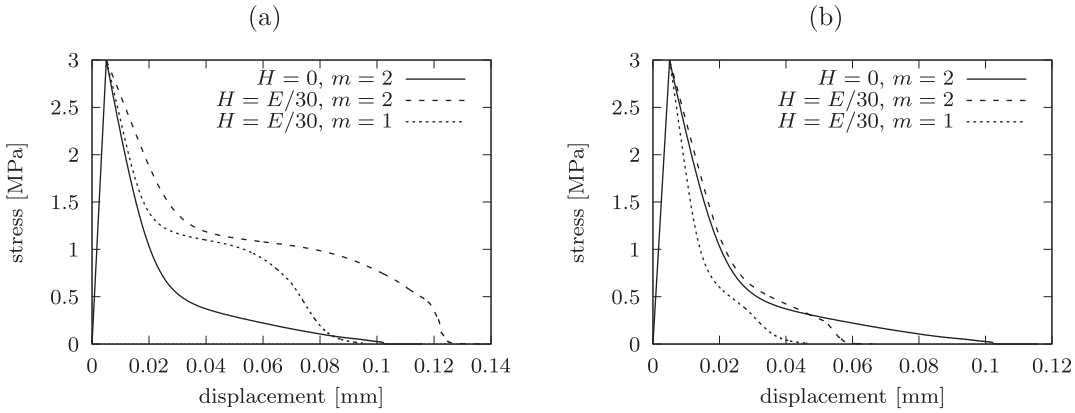

Fig. 12. Stress-displacement diagrams for DPM, obtained using (a) double-exponential law (62) with $a = 1200$, $a_2 = 120$ and $c_2 = 0.2$, and (b) double-exponential law (64) with $\varepsilon_f = 0.9333 \cdot 10^{-3}$, $\varepsilon_{f2} = 8.4333 \cdot 10^{-3}$ and $c_2 = 0.2$.

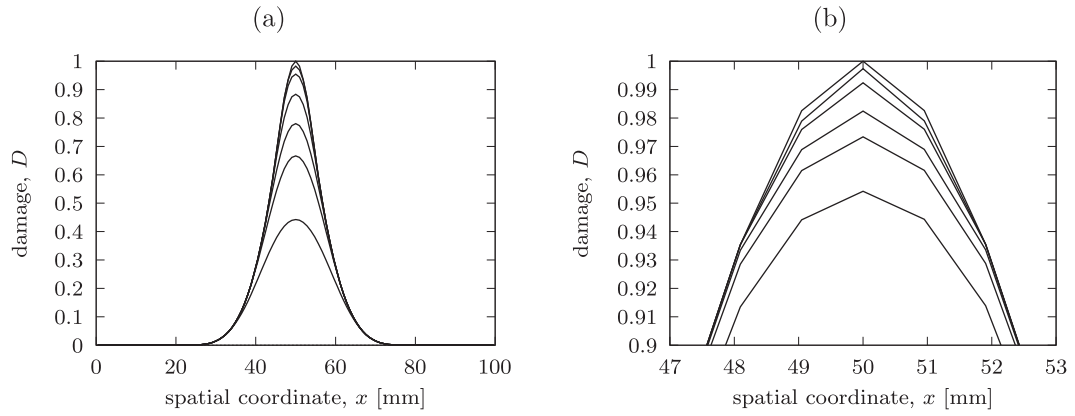

Fig. 13. Evolution of damage profiles for DPM with double-exponential law (64) and parameters $H = E/30$, $m = 1$, $\varepsilon_f = 0.9333 \cdot 10^{-3}$, $\varepsilon_{f2} = 8.4333 \cdot 10^{-3}$ and $c_2 = 0.2$.

$1/a_2$. If the modified formula (64) is used, the bumps become less dramatic but do not completely disappear; see the dashed and dotted curves in Fig. 12b. A potential advantage of the formulation with $H > 0$ is that the damage profiles no longer have a central flat part; see Fig. 13a. The active part of the damage zone is shrinking but even at very advanced stages of the damage process contains several elements; see Fig. 13b.

Possible extensions to the pure damage model are analyzed in Appendix C. It is shown that a modified damage law that corresponds to a double-exponential local softening curve would lead to wavy shapes of the stress-displacement diagrams, but a law that corresponds to a properly constructed power-exponential local softening curve can provide, for a specific choice of parameters, a reasonably shaped stress-displacement diagram with a tail.

6. Summary and concluding remarks

We have performed a one-dimensional localization analysis of three families of nonlocal softening models suitable for quasi-brittle materials such as concrete, for which the resulting equivalent cohesive curves are supposed to exhibit a long tail similar to the experimental data plotted in Fig. 2b. The three considered families of constitutive models were: (i) pure damage models (DM) with no permanent strain, (ii) damage-plastic models (DPM) with permanent strain obtained from plasticity formulated in the effective stress space and with damage driven by the plastic flow, and (iii) models with damage-driven inelastic strains (DMIS), for which the permanent strains are directly related to damage.

A nonlocal integral (1D) formulation in which the nonlocal interactions are made damage-dependent by using the effective distance defined in (1) has been considered. For this formulation, the computations are found to be mesh-independent, both plastic strain and damage remain localized in a narrow band, and the full damage ($D = 1$) is localized at a single point. The computation of the effective distance $\tilde{r}$ between interacting points is made robust thanks to the proposed integration scheme (59). An interesting theoretical issue is the precise limiting shape of the damage profile in the uniaxial bar when the displacement tends to infinity and the stress to zero. This point is briefly discussed in Appendix B.

We have focused our attention on the role of permanent strains and on localization properties of formulations that exploit them. We have shown that the dramatic snapback accompanied by loss of convexity of the softening branch of the global stress-displacement diagram for a bar under uniaxial tension, which occurs for pure damage models (with no permanent strain at all), can be changed into a long tail by accounting for permanent strains. More promising results have been obtained for plasticity-driven permanent strains (DPM) than for damage-driven inelastic strains (DMIS). The present study identifies the formulations that are suitable candidates for extensions of the model to multiple dimensions, in which the evaluation of the effective distance is computationally more demanding.

One could also envision an alternative remedy, based on an adjustment of the function used in the damage law. When properly formulated, such modification can extend the tail of the local stress-strain diagram and a similar effect can be expected on the global response, characterized by the load-displacement diagram under uniaxial tension. For the damage-plastic model, the replacement of an exponential function by the sum of two exponential functions can lead to very promising results, as demonstrated in

Section 5. An attempt to design a similar modification for the pure damage model is documented in Appendix C. In this case, using a sum of two exponential function does not lead to very satisfactory results, but an improvement is achieved with a specific form of a power-exponential law. The robustness of such modifications needs to be checked in multiple dimensions, which is the subject of ongoing work.

The class of pure damage models examined in this paper directly links damage to strain, which is fully sufficient in the one-dimensional context. For general multi-axial stress, a variety of damage formulations could be considered, e.g., models with multiple scalar damage variables and anisotropic models dealing with damage tensors. In many cases, the damage law loses its explicit character, either because it is written in the rate form, or because the loading-unloading conditions are postulated in terms of stress. For instance, the so-called bi-dissipative model for concrete proposed by Comi and Perego (2001) uses separate damage variables for tension and for compression and deals with stress-based loading-unloading conditions. The damage evaluation algorithm is then no longer explicit and requires iterations, similar to stress-return algorithms in plasticity. However, since stress is uniquely determined by strain and damage, the loading functions can be rewritten as functions of strain and damage and the conditions can be reformulated in the strain space. Under uniaxial stress, this is fully equivalent to the strain-driven damage model considered in the present study. It is worth noting that when the bi-dissipative model for concrete was extended to a nonlocal formulation (Comi, 2001), the loading functions were transformed to the strain space and nonlocal averaging was applied to strain invariants, which corresponds to the standard nonlocal damage framework.

Acknowledgement

Financial support received from the Czech Science Foundation (GAČR project No. 17-04150J) is gratefully acknowledged.

Appendix A. Functions g_{dis} and α_{dis} for Various Versions of DMIS

In this appendix, we present a detailed derivation of the specific form of functions g_{dis} and α_{dis} used by the damage model with inelastic strain. An overview of these functions was provided in Table 1.

Version 1. It is assumed that the unloading slope is the same as for the DPM with linear hardening of the plastic part. From (28) we obtain

$$\begin{aligned} g_{dis}(\varepsilon) &= g_{dp}(\varepsilon_p(\varepsilon)) = 1 - \frac{f_t}{f_t + H\varepsilon_p(\varepsilon)} \exp\left(-\frac{(1+H/E)\varepsilon_p(\varepsilon)}{\varepsilon_f - \varepsilon_0}\right) \\ &= 1 - \frac{f_t}{f_t + H(E\varepsilon - f_t)/(E+H)} \exp\left(-\frac{\varepsilon - \varepsilon_0}{\varepsilon_f - \varepsilon_0}\right) \\ &= 1 - \frac{1}{1 + (E_{ep}/E)(\varepsilon/\varepsilon_0 - 1)} \exp\left(-\frac{\varepsilon - \varepsilon_0}{\varepsilon_f - \varepsilon_0}\right) \end{aligned} \tag{65}$$

where $E_{ep} = EH/(E+H)$ is the elastoplastic modulus of the plastic part of the model.

For a nonzero plastic modulus H, function g_{dis} given by (65) is not invertible in closed form. In fact, this function is not really needed, because the inelastic strain can be evaluated from the damage-driving variable κ_d instead of from the damage D. Eqs. (18)–(19) can be combined into

$$\varepsilon_p = \alpha_{dis}(g_{dis}(\kappa_d)) \equiv \beta_{dis}(\kappa_d) \tag{66}$$

and function β_{dis} is in general given by the right-hand side of (28), which in the present case leads to

$$\begin{aligned} \beta_{dis}(\varepsilon) &= \varepsilon - \frac{\sigma_d(\varepsilon)}{E[1 - g_{dis}(\varepsilon)]} \\ &= \varepsilon - \frac{f_t \exp\left(-\dfrac{\varepsilon - \varepsilon_0}{\varepsilon_f - \varepsilon_0}\right)}{\dfrac{E}{1 + (E_{ep}/E)(\varepsilon/\varepsilon_0 - 1)} \exp\left(-\dfrac{\varepsilon - \varepsilon_0}{\varepsilon_f - \varepsilon_0}\right)} \\ &= \varepsilon - [\varepsilon_0 + (E_{ep}/E)(\varepsilon - \varepsilon_0)] = \frac{E}{E+H}(\varepsilon - \varepsilon_0) \end{aligned} \tag{67}$$

Version 1s. In the special case with $H = 0$, formula (65) simplifies to

$$g_{dis}(\varepsilon) = 1 - \exp\left(-\frac{\varepsilon - \varepsilon_0}{\varepsilon_f - \varepsilon_0}\right) \tag{68}$$

and becomes invertible in an analytical form. The inverse function is then

$$g_{dis}^{-1}(D) = \varepsilon_0 - (\varepsilon_f - \varepsilon_0)\ln(1 - D) \tag{69}$$

In this case, we can apply formula (30) directly and construct an explicit expression for function α_{dis}. After easy manipulations we obtain

$$\alpha_{dis}(D) = g_{dis}^{-1}(D) - \frac{\sigma_d(g_{dis}^{-1}(D))}{E(1-D)} = -(\varepsilon_f - \varepsilon_0)\ln(1 - D) \tag{70}$$

Version 2s. Instead of matching the damage model with inelastic strain to the damage-plastic model, we can match the monotonic stress-strain curve only and postulate the dependence of inelastic strain on damage separately. This approach gives a different type of unloading behavior. Once we postulate the form of function α_{dis}, we can identify function g_{dis} from (27). For instance, if it is assumed that the inelastic strain is proportional to damage, we set

$$\alpha_{dis}(D) = \alpha D \tag{71}$$

where α is a given constant. Eq. (27) then becomes

$$[1 - g_{dis}(\varepsilon)]\, E\, [\varepsilon - \alpha g_{dis}(\varepsilon)] = \sigma_d(\varepsilon) \tag{72}$$

which is a quadratic equation with two positive roots. It can be verified that the correct root is the smaller one,

$$g_{dis}(\varepsilon) = \frac{\varepsilon + \alpha - \sqrt{(\varepsilon + \alpha)^2 - 4\alpha[\varepsilon - \sigma_d(\varepsilon)/E]}}{2\alpha} \tag{73}$$

Indeed, at the onset of damage we have $\varepsilon = \varepsilon_0$ and $\sigma_d(\varepsilon) = E\varepsilon$, and formula (73) gives $g_{dis}(\varepsilon_0) = 0$, i.e., zero damage. As ε tends to infinity, $\sigma_d(\varepsilon)$ tends to zero and g_{dis} approaches 1 from below.

Version 2. For nonlinear functions α_{dis}, the corresponding function g_{dis} usually cannot be constructed analytically, but its values can always be computed numerically. Denoting $g_{dis}(\varepsilon)$ as D, we can rewrite (27) as

$$(1 - D)[\varepsilon - \alpha_{dis}(D)] = \frac{\sigma_d(\varepsilon)}{E} \tag{74}$$

or, equivalently, as

$$F(D) \equiv D\alpha_{dis}(D) - \alpha_{dis}(D) - D\varepsilon + \varepsilon - \frac{\sigma_d(\varepsilon)}{E} = 0 \tag{75}$$

This nonlinear equation is solved by the Newton method, starting from the initial approximation $D_0 = 0$, for which $F(D_0) = \varepsilon - \sigma_d(\varepsilon)/E \geq 0$. The derivative of F is given by

$$F'(D) = \alpha_{dis}(D) + D\alpha'_{dis}(D) - \alpha'_{dis}(D) - \varepsilon \tag{76}$$

and so $F'(D_0) = -\alpha'_{dis}(D) - \varepsilon < 0$. The recursive algorithm

$$D_k = D_{k-1} - \frac{F(D_{k-1})}{F'(D_{k-1})}, \qquad k = 1, 2, \dots \tag{77}$$

should converge to a limit D which represents the value of $g_{dis}(\varepsilon)$. As a specific case, we consider

$$\alpha_{dis}(D) = \alpha D^p \tag{78}$$

where p is a fixed exponent. Then we have

$$F(D) = \alpha D^{p+1} - \alpha D^p - \varepsilon D + \varepsilon - \frac{\sigma_d(\varepsilon)}{E} \tag{79}$$

$$F'(D) = (p+1)\alpha D^p - p\alpha D^{p-1} - \varepsilon \tag{80}$$

Version 3. One special case in which function α_{dis} is nonlinear but the problem can still be treated analytically is the choice

$$\alpha_{dis}(D) = \alpha \frac{D}{1-D} \tag{81}$$

Eq. (74) can then be rewritten as

$$(1-D)\left[\varepsilon - \alpha \frac{D}{1-D}\right] = \frac{\sigma_d(\varepsilon)}{E} \tag{82}$$

which is equivalent to the linear equation

$$(1-D)\varepsilon - \alpha D = \frac{\sigma_d(\varepsilon)}{E} \tag{83}$$

and the solution can be written in closed form as

$$D = \frac{\varepsilon - \sigma_d(\varepsilon)/E}{\varepsilon + \alpha} \equiv g_{dis}(\varepsilon) \tag{84}$$

It is then easy to evaluate the inelastic strain

$$\varepsilon_p = \alpha \frac{D}{1-D} = \alpha \frac{E\varepsilon - \sigma_d(\varepsilon)}{E\alpha + \sigma_d(\varepsilon)} \equiv \beta_{dis}(\varepsilon) \tag{85}$$

Appendix B. Shape of Ultimate Damage Profile

An interesting theoretical issue is the precise shape of the damage profile that is approached in the limit as the displacement tends to infinity and the stress to zero. It is clear that damage at the center of the process zone tends to 1, but is the spatial derivative of damage at this point equal to zero, or is it discontinuous?

Let us place the center of the process zone to the origin ($x = 0$). If the limit damage profile is smooth, the leading term in the expansion of $1 - D(x)$ around the origin is quadratic, and we have

$$D(x) \approx 1 + \frac{1}{2}D''(0)x^2 \tag{86}$$

where $D''(0) < 0$. The integral of $1/\sqrt{1-D}$ then becomes singular at $x = 0$, because

$$\int \frac{\mathrm{d}x}{\sqrt{1-D(x)}} \approx \int \frac{\mathrm{d}x}{\sqrt{-D''(0)x^2/2}} = \sqrt{\frac{2}{-D''(0)}} \int \frac{\mathrm{d}x}{|x|} \tag{87}$$

The modified distance between the origin and any other point is then infinite and no interaction takes place across the center of the damage zone.

On the other hand, if the limit damage profile has a kink at the origin, it can be approximated by

$$D(x) \approx 1 + D'(0^+)|x| \tag{88}$$

where $D'(0^+) < 0$, and function $1/\sqrt{1-D}$ is then integrable:

$$\int \frac{\mathrm{d}x}{\sqrt{1-D(x)}} \approx \int \frac{\mathrm{d}x}{\sqrt{-D'(0^+)x}} = \frac{1}{\sqrt{-D'(0^+)}} \int \frac{\mathrm{d}x}{\sqrt{|x|}} = \frac{2\,\mathrm{sgn}\,x\sqrt{|x|}}{\sqrt{-D'(0^+)}} \tag{89}$$

In this case, the modified distance is increased but still finite, and points that are sufficiently close can interact even across the center of the damage zone.

Appendix C. Damage Model with Double-Exponential or Power-Exponential Law

In Section 5 it was shown that the tail of the stress-displacement diagram obtained with the damage-plastic model can be extended by reformulating the damage law. Modifications of the exponential softening law can also improve the shape of the stress-displacement diagrams for the pure damage model. The **double-exponential** stress-strain relation (63) corresponds to the damage function of the pure damage model defined as

$$g_d(\kappa_d) = 1 - \frac{\sigma_d(\kappa_d)}{E\kappa_d} = 1 - \frac{\varepsilon_0}{\kappa_d}\left[(1-c_2)\exp\left(-\frac{\kappa_d - \varepsilon_0}{\varepsilon_f - \varepsilon_0}\right) + c_2 \exp\left(-\frac{\kappa_d - \varepsilon_0}{\varepsilon_{f2} - \varepsilon_0}\right)\right] \tag{90}$$

The curves plotted in Fig. 14a have been obtained with parameters $\varepsilon_f = 3 \cdot 10^{-4}$ and $\varepsilon_{f2} = 3 \cdot 10^{-3}$ and with c_2 ranging from 0 to 0.4. As the value of c_2 is increased, the response becomes less brittle but the softening curves have a wavy shape, which is especially apparent for fine meshes. When ε_f and ε_{f2} are increased, the curves retain the wavy shape; see Fig. 14b.

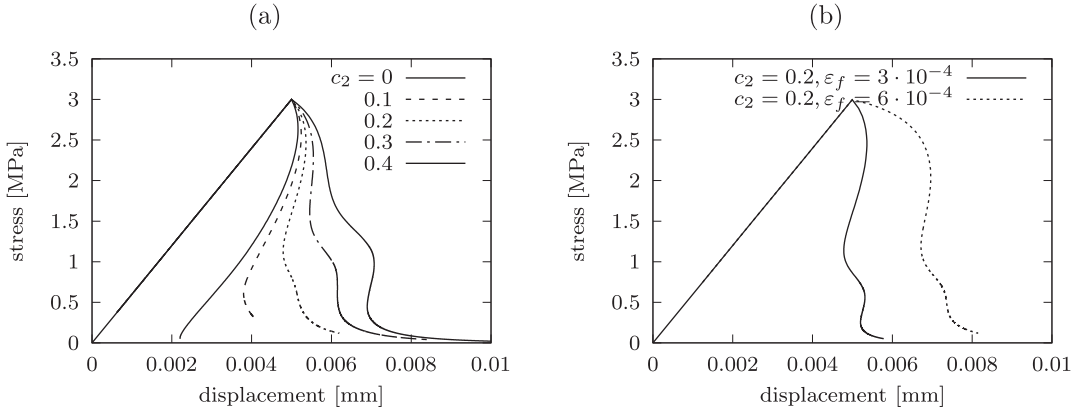

Fig. 14. Stress-displacement diagrams for the damage model with the double-exponential law (90): (a) parameters $\varepsilon_f = 3 \cdot 10^{-4}$ and $\varepsilon_{f2} = 3 \cdot 10^{-3}$ fixed, parameter c_2 varied, (b) parameter $c_2 = 0.2$ fixed, parameters ε_f and $\varepsilon_{f2} = 10\,\varepsilon_f$ varied.

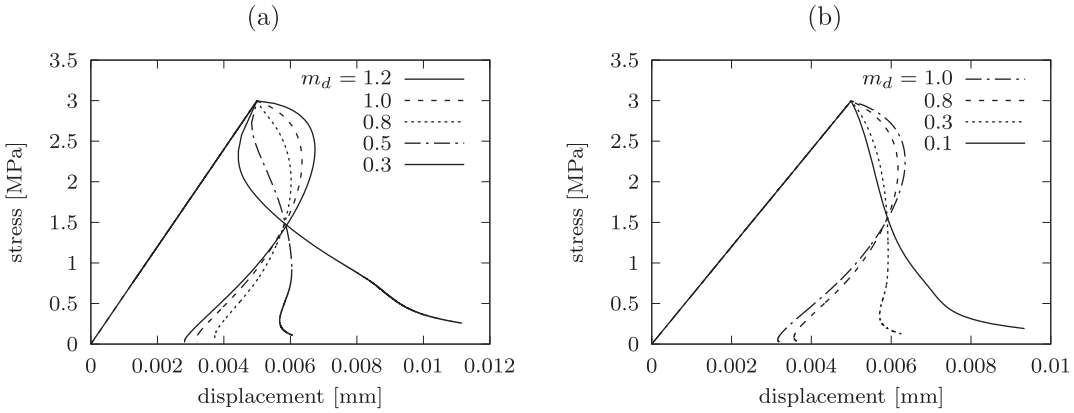

Fig. 15. Stress-displacement diagrams for the damage model with a power-exponential law (a) given by (91), (b) given by (92).

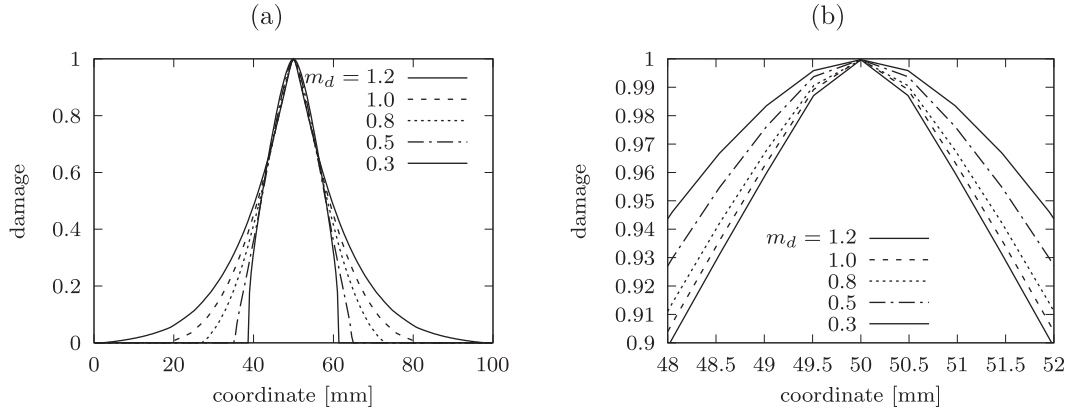

Fig. 16. Ultimate damage profiles for the damage model with power-exponential law (91).

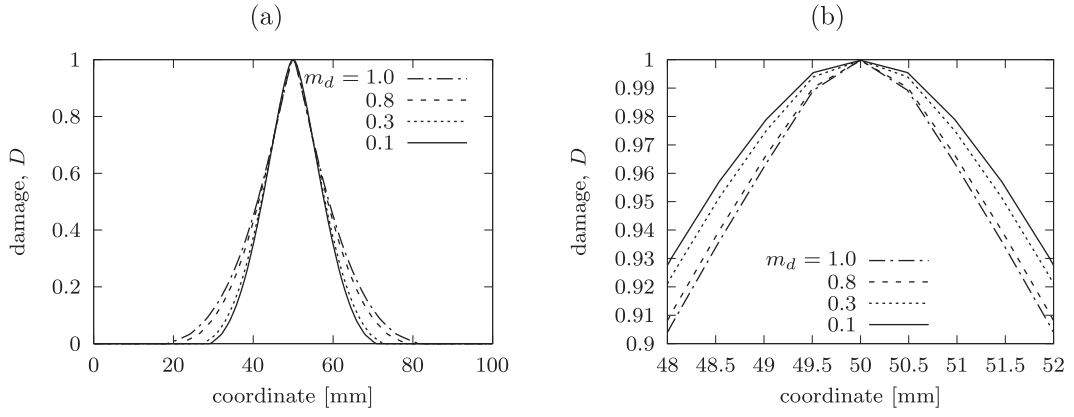

Fig. 17. Ultimate damage profiles for the damage model with power-exponential law (92).

The response can be made more ductile not only by adding a slowly decaying exponential, but also by raising the argument of the exponential to a power. The **power-exponential** damage law

$$g_d(\kappa_d) = 1 - \frac{\varepsilon_0}{\kappa_d} \exp\left(-\left(\frac{\kappa_d - \varepsilon_0}{\varepsilon_f - \varepsilon_0}\right)^{m_d}\right) \tag{91}$$

uses an adjustable exponent m_d, and for $m_d = 1$ reduces to (90). As m_d is decreased, the stress-displacement curve changes shape from concave to convex; see Fig. 15a. A tail is obtained for $m_d = 0.3$ but the response is very brittle right after the peak and the curve exhibits a sharp snapback, only later changing into almost linear softening and a tail. The brittleness right after peak is certainly related to the fact that, for $m_d < 1$, the local stress-strain curve starts at the peak with a vertical slope. This undesirable effect can be removed by reformulating the power-exponential law such that the value of the variable that is raised to m_d is not 0 at the onset of damage. A suitable formula is

$$g_d(\kappa_d) = 1 - \frac{\varepsilon_0}{\kappa_d} \exp\left(-\frac{\kappa_d^{m_d} - \varepsilon_0^{m_d}}{\varepsilon_f^{m_d} - \varepsilon_0^{m_d}}\right) \tag{92}$$

With this damage law, quite a reasonable shape of the stress-displacement curve can be obtained if m_d is set to 0.1; see the solid curve in Fig. 15b.

Damage profiles corresponding to the last computed step are plotted in Fig. 16 for the model with damage law (91) and in Fig. 17 for the model with damage law (92). In both cases,

reduction of exponent m_d leads to more narrow damage profiles that are more rounded around the center of the damage zone (than in the standard case of $m_d = 1$).

References

Bažant, Z.P., 1990. Why continuum damage is nonlocal: micromechanics arguments. J. Eng. Mech. 117, 1070–1087.

Bažant, Z.P., 1994. Nonlocal damage theory based on micromechanics of crack interactions. J. Eng. Mech. 120, 593–617.

Bažant, Z.P., Jirásek, M., 1994. Damage nonlocality due to microcrack interactions: statistical determination of crack influence function. In: Bažant, Z.P., Bittnar, Z., Jirásek, M., Mazars, J. (Eds.), Fracture and Damage in Quasibrittle Structures. E & FN Spon, London UK, pp. 3–17.

Bažant, Z.P., Jirásek, M., 2002. Nonlocal integral formulations of plasticity and damage: survey of progress. J. Eng. Mech. 128, 1119–1149.

Bažant, Z.P., Le, J., Hoover, C., 2010. Nonlocal boundary layer (NBL) model: overcoming boundary condition problems in strength statistics and fracture analysis of quasibrittle materials. In: FraMCoS-7, Korea, pp. 135–143.

Bažant, Z.P., Pijaudier-Cabot, G., 1988. Nonlocal continuum damage. J. Eng. Mech. 55, 287–293.

Belytschko, T., Krongauz, Y., Organ, D., Fleming, M., Krysl, P., 1996. Meshless methods: an overview and recent developments. Comput. Method Appl. Mech.Eng. 139, 3–47.

Belytschko, T., Lu, Y., Gu, L., 1995. Crack propagation by element-free Galerkin methods. Eng. Fract. Mech. 51, 295–315.

Borderie, C.L., 1991. Phénomènes Unilatéraux Dans un Matériau Endommageable. Université Paris 6, France Ph.D. thesis.

Borino, G., Failla, B., Parrinello, F., 2003. A symmetric nonlocal damage theory. Int. J. Solids Struct. 40, 3621–3645.

Burlion, N., Gatuingt, F., Pijaudier-Cabot, G., Daudeville, L., 2000. Compaction and tensile damage in concrete: constitutive modelling and application to dynamics. Comput. Methods Appl. Mech. Eng. 183, 291–308.

Chen, H.H., Su, R.K.L., 2013. Tension softening curves of plain concrete. Constr. Build. Mater. 44, 440–451.

Comi, C., 2001. Non-local model with tension and compression damage mechanisms. Eur. J. Mech. A/Solids 20 (1), 1–22.

Comi, C., Perego, U., 2001. Fracture energy based bi-dissipative damage model for concrete. Int. J. Solids Struct. 38, 6427–6454.

Desmorat, R., 2004. Modèle d'endommagement anisotrope avec forte dissymétrie traction/compression. 5è journées du Regroupement Francophone pour la Recherche et la Formation sur le Béton (RF2B), 5–6 July, Liège, Belgium.

Desmorat, R., Gatuingt, F., 2007. Introduction of an Internal Time in Nonlocal Integral Theories. http://hal.archives-ouvertes.fr/hal-00200898/en/

Desmorat, R., Gatuingt, F., 2010. Introduction of an internal time in nonlocal integral theories. In: Computational Modelling of Concrete Structures, pp. 121–128. doi:10.1201/b10546-15.

Desmorat, R., Gatuingt, F., Jirásek, M., 2015. Nonlocal models with damage-dependent interactions motivated by internal time. Eng. Fract. Mech. 142, 255–275. doi:10.1016/j.engfracmech.2015.06.015.

Desmorat, R., Gatuingt, F., Ragueneau, F., 2010. Nonstandard thermodynamics framework for robust computations with induced anisotropic damage. Int. J. Damage Mech. 19, 53–73.

Feenstra, P., Borst, R.D., 1996. A composite plasticity model for concrete. Int. J. Solids Struct. 33, 707–730.

Frémond, M., Nedjar, B., 1996. Damage, gradient of damage and principle of virtual power. Int. J. Solids Struct. 33, 1083–1103.

Geers, M.G.D., de Borst, R., Brekelmans, W.A.M., Peerlings, R.H.J., 1998. Strain-based transient gradient damage model for failure analysis. Comput. Methods Appl. Mech. Eng. 160, 133–154.

Giry, C., Dufour, F., Mazars, J., 2011. Stress-based nonlocal damage model. Int. J. Solids Struct. 48, 3431–3443.

Gopalaratnam, V.S., Shah, S.P., 1985. Softening response of plain concrete in direct tension. J. Am. Concr. Inst. 82, 310–323.

Govindjee, S., Kay, G., Simo, J., 1995. Anisotropic modelling and numerical simulation of brittle damage in concrete. Int. J. Numer. Methods Eng. 38, 3611–3633.

Grassl, P., Jirásek, M., 2006. Damage-plastic model for concrete failure. Int. J. Solids Struct. 43, 7166–7196.

Grassl, P., Jirásek, M., 2006. Plastic model with non-local damage applied to concrete. Int. J. Numer. Anal. Methods Geomech. 30 (1), 71–90. doi:10.1002/nag.479.

Grégoire, D., Rojas-Solano, L., Pijaudier-Cabot, G., 2013. Failure and size effect for notched and unnotched concrete beams. Int. J. Numer. Anal. Methods 37, 1434–1452.

Halm, D., Dragon, A., 1998. An anisotropic model of damage and frictional sliding for brittle materials. Eur. J. Mech.-A/Solids 17, 439–460.

Hermann, G., Kestin, J., 1988. On the thermodynamics foundation of a damage theory in elastic solids. In: Cracking and damage, pp. 228–232.

Hordijk, D.A., 1991. Local Approach to Fatigue of Concrete. Delft University of Technology, Delft, The Netherlands Ph.D. thesis.

Jirásek, M., Rolshoven, S., 2003. Comparison of integral-type nonlocal plasticity models for strain-softening materials. Int. J. Eng. Sci. 41 (13–14), 1553–1602. doi:10.1016/S0020-7225(03)00027-2.

Jirásek, M., Rolshoven, S., Grassl, P., 2004. Size effect on fracture energy induced by non-locality. Int. J. Numer. Anal. Methods 28, 653–670.

Krayani, A., Pijaudier-Cabot, G., Dufour, F., 2009. Boundary effect on weight function in nonlocal damage model. Eng. Fract. Mech. 76, 2217–2231.

Lebon, G., 2011. Analyse de L'endommagement des Structures de Génie Civil: Techniques de Sous-Structuration Hybride Couplées á un modèle D'endommagement Anisotrope. ENS-Cachan, France Ph.D. thesis.

Lee, S.-K., Woo, S.-K., Song, Y.-C., 2008. Softening response properties of plain concrete by large-scale direct tension tests. Mag. Concr. Res. 60 (1), 33–40.

Lemaitre, J., Chaboche, J.-L., 1985. Mécanique des Matériaux Solides. Dunod, English Translation 1990 'Mechanics of Solid Materials' Cambridge University Press.

Marigo, J.-J., 1981. Formulation d 'une loi d 'endommagement d'un matériau élastique. Compt. Rend. l'Acad. Sci. Sér. II 292, 1309–1312.

Matallah, M., Borderie, C.L., 2009. Inelasticity-damage-based model for numerical modeling of concrete cracking. Eng. Fract. Mech. 76, 1087–1108.

Mazars, J., 1984. Application de la Mécanique de L'endommagement au Comportement non Linéaire et à la Rupture du Béton de Structure. Thèse de Doctorat d'Etat. Université Paris VI., France.

Mazars, J., Berthaud, Y., Ramtani, S., 1990. The unilateral behavior of damage concrete. Eng. Fract. Mech. 76, 629–635.

Mazars, J., Ramtani, S., Berthaud, Y., 1989. An experimental procedure to delocalize tensile failure and to identify unilateral effect of distributed damage. In: Mazars, J., Bažant, Z.P. (Eds.), Cracking and damage: strain localization and size effect. Elsevier, London UK, pp. 55–64.

Meschke, G., Lackner, R., Mang, A., 1998. An anisotropic elastoplastic-damage model for plain concrete. Int. J. Numer. Methods Eng. 42, 703–727.

Miehe, C., Welschinger, F., Hofacker, M., 2010. Thermodynamically consistent phase–field models of fracture: variational principles and multi-field fe implementations. Int. J. Numer. Methods Eng. 83, 1273–1311.

Nechnech, W., Meftah, F., Reynouard, J., 2002. An elasto-plastic damage model for plain concrete subjected to high temperatures. Eng. Struct. 24, 597–611.

Nguyen, G.D., 2011. A damage model with evolving nonlocal interactions. Int. J. Solids Struct. 48, 1544–1559.

Peerlings, R., De Borst, R., Brekelmans, W., De Vree, J., Spee, I., 1996. Some observations on localisation in non-local and gradient damage models. Eur. J. Mech. A 15, 937–953.

Pijaudier-Cabot, G., Bažant, Z.P., 1987. Nonlocal damage theory. J. Eng. Mech. 113, 1512–1533.

Pijaudier-Cabot, G., Benallal, A., 1993. Strain localization and bifurcation in a nonlocal continuum. Int. J. Solids Struct. 30, 1761–1775.

Pijaudier-Cabot, G., Dufour, F., 2010. Non local damage model: boundary and evolving boundary effects. Eur. J. Environ. Civil Eng. 14, 729–749.

Pijaudier-Cabot, G., Haidar, K., Dubé, J.-F., 2004. Non-local damage model with evolving internal length. Int. J. Numer. Anal. Methods. Geomech. 28, 633–652.

Ragueneau, F., Borderie, C.L., Mazars, J., 2000. Damage model for concrete-like materials coupling cracking and friction, contribution towards structural damping: first uniaxial applications. Mech. Cohes-Frict. Mater. 5, 607–626.

Rastiello, G., Giry, C., Gatuingt, F., Desmorat, R., 2018. From diffuse damage to strain localization from an Eikonal Non-Local (ENL) Continuum Damage model with evolving internal length. Comput. Methods Appl. Mech. Eng. 331, 650–674. doi:10.1016/j.cma.2017.12.006.

Rojas-Solano, L., Grégoire, D., Pijaudier-Cabot, G., 2013. Interaction-based non-local damage model for failure in quasi-brittle materials. Mech. Res. Commun. 54, 56–62.

Saroukhani, S., Vafadari, R., Simone, A., 2013. A simplified implementation of a gradient-enhanced damage model with transient length scale effects. Comput. Mech. 51, 899–909.

Simone, A., Askes, H., Sluys, L.J., 2004. Incorrect initiation and propagation of failure in non-local and gradient-enhanced media. Int. J. Solids Struct. 41, 351–363.

Simone, A., Wells, G.N., Sluys, L.J., 2003. From continuous to discontinuous failure in a gradient-enhanced continuum damage model. Comput. Methods Appl. Mech. Eng. 192, 4581–4607.

Strömberg, L., Ristinmaa, M., 1996. FE-formulation of a nonlocal plasticity theory. Comput. Methods Appl. Mech. Eng. 136, 127–144.

Sun, G., Poh, L., 2016. Homogenization of intergranular fracture towards a transient gradient damage model. J. Mech. Phys. Solids 95, 374–392.

Terrien, M., 1980. Emission Acoustique et Comportement Mécanique Post-Critique d'un Béton Sollicité en Traction. Bulletin de Liaison du LCPC. 105

Valentini, B., Hofstetter, G., 2013. Review and enhancement of 3D concrete models for large-scale numerical simulations of concrete structures. Int. J. Numer. Anal. Meth. Geomech. 37, 221–246.

Vermeer, P.A., Brinkgreve, R.B.J., 1994. A new effective non-local strain measure for softening plasticity. In: Chambon, R., Desrues, J., Vardoulakis, I. (Eds.), Localisation and Bifurcation Theory for Soils and Rocks. Balkema, Rotterdam, pp. 89–100.

de Vree, J.H.P., Brekelmans, W.A.M., van Gils, M.A.J., 1995. Comparison of nonlocal approaches in continuum damage mechanics. Comput. Struct. 55, 581–588.